Experimental and Theoretical Study of Phonon Scattering from Simple Point Defects in Sodium Chloride*

R. F. CALDWELL† AND MILES V. KLEIN
Department of Physics and Materials Research Laboratory, University of Illinois, Urbana, Illinois
(Received 7 November 1966)

Thermal-conductivity measurements have been made as a function of temperature on sodium chloride crystals containing the nine monovalent substitutional impurities: F^-, Br^-, I^-, Li^+, K^+, Rb^+, Ag^+, Tl^+, and Cu^+. These measurements extend over the temperature range 1.2 to 300°K. All of the systems showed a lowering of the curves which is asymmetric which respect to the peak. In order to explain this behavior, the Debye approximation in the expression for the thermal-conductivity integral has been relaxed. Phonon data were calculated using the shell model for 64 000 points in the Brillouin zone. From these data a density of states and frequency-averaged group velocities were obtained and then used in the conductivity integral. In addition, exact relaxation rates were obtained, via a Green's-function formalism derived by Klein, for a simple model for the defect in the lattice, which assumed a change of mass at the defect site and a change of force constant to the six nearest neighbors. The changes in force constant were obtained using a Born-Meyer repulsive potential between the ions. New equilibrium positions of the surrounding ions were obtained from published literature and from a method using the static Green's functions. The results for the change in force constant varied considerably, so that this parameter was considered to be semivariable in the analysis. Depressions of the conductivity curve were predicted at approximately the same positions as found experimentally. The predicted high-temperature depressions occurred at slightly lower temperatures than the experimental ones and the strengths did not agree very well with experiment. The degree to which the theory successfully predicted the experimental curves is related to the size of the strain field about the impurity. Thus it is hoped that a more sophisticated model containing long-range effects will improve the fit.

I. INTRODUCTION

THE work described in this paper was undertaken to make a systematic study of the scattering of phonons from monovalent substitutional impurities in sodium chloride. Nine impurities were studied: flourine, bromine, iodine, lithium, potassium, rubidium, silver, thallium, and copper.

Experimentally, the scattering of phonons can be observed by measurements of the lattice thermal conductivity. Despite some rather severe problems in analyzing the data, this is a good tool to use since at low temperatures defects in the lattice have a strong influence on the thermal conductivity. Review articles on this topic have been written by Klemens[1] and Carruthers.[2] At the present time, the most fruitful method of analysis is one advanced by Callaway[3] which is valid within the Debye approximation for the phonons and which uses a relaxation-time approach.

A number of workers have made lattice thermal-conductivity measurements at low temperatures on alkali-halide crystals containing point defects such as F centers,[4] isotopes,[5,6] vacancies,[7] substitutional divalent impurities,[8–10] and substitutional monovalent impurities.[10–14] With the exception of the isotope results, all of these systems show non-Rayleigh scattering, i.e., depressions in the thermal-conductivity curves which are asymmetric with respect to the peak. The Rayleigh scattering laws were derived by Klemens[15] within the Debye and long-wavelength approximations.

Some thermal-conductivity work has already been done at higher temperatures on some of the same systems which we have studied, viz., NaCl containing Ag^+, Br^-, and K^+ in the temperature range 100 to 380°K[16] and NaCl containing Li^+, I^-, and Rb^+ at room temperature.[17]

Phonon scattering from point defects has been studied from a theoretical standpoint by a number of people beginning with Lifshitz.[18] The most extensively studied model has been that of a change of mass at the defect

* This research was supported in part by the Advanced Research Projects Agency under Contract No. SD-131, by the U. S. Atomic Energy Commission under Contract No. AT(11-1)-1198 (Report No. COO-1198-390), and also by the A. P. Sloan Foundation.

† Present address: Eastman Kodak Company, Apparatus and Optical Division Research Laboratories, Rochester, New York.

[1] P. G. Klemens, in *Solid-State Physics*, edited by F. Seitz and D. Turnbull (Academic Press Inc., New York, 1958), Vol. 7, p. 1.

[2] P. Carrauthers, Rev. Mod. Phys. **33**, 92 (1961).

[3] J. Callaway, Phys. Rev. **113**, 1046 (1959).

[4] R. O. Pohl, Phys. Rev. **118**, 1499 (1960).

[5] P. D. Thatcher, Ph.D. dissertation, Cornell University, 1965 (unpublished).

[6] R. Berman and J. C. F. Brock, Proc. Roy. Soc. (London) **A289**, 46 (1965).

[7] J. W. Schwartz and C. T. Walker, Phys. Rev. Letters **16**, 97 (1966).

[8] G. A. Slack, Phys. Rev. **105**, 832 (1957).

[9] M. V. Klein, Phys. Rev. **123**, 1977 (1961).

[10] C. T. Walker and R. O. Pohl, Phys. Rev. **131**, 1433 (1963).

[11] W. S. Williams, Phys. Rev. **119**, 1921 (1960).

[12] J. M. Worlock, Phys. Rev. **147**, 636 (1966).

[13] F. C. Baumann, Bull. Am. Phys. Soc. **9**, 644 (1964).

[14] R. O. Pohl (private communication).

[15] P. G. Klemens, Proc. Roy. Soc. (London) **A68**, 1113 (1955).

[16] E. D. Devyatkova, M. I. Kornfel'd, and I. A. Smirnov, Zh. Eksperim. i Teor. Fiz. **42**, 307 (1962) [English transl.: Soviet Phys.—JETP **15**, 212 (1962)].

[17] E. D. Devyatkova, M. I. Kornfel'd, and I. A. Smirnov, Fiz. Tverd. Tela **4**, 3669 (1962) [English transl.: Soviet Phys.—Solid State **4**, 2683 (1963)].

[18] I. M. Lifshitz, Zh. Eksperim. i Teor. Fiz. **18**, 293 (1948); Nuovo Cimento **3**, 716 (1956).

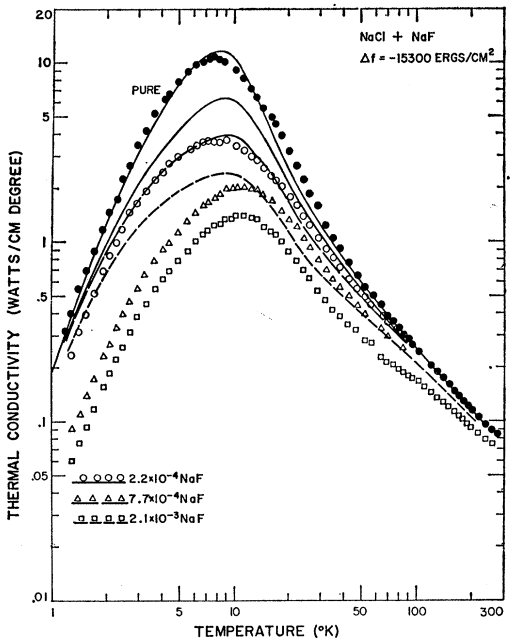

FIG. 1. Thermal conductivity of the system NaCl:NaF. Points are the experimental data and the lines are the theoretical fits.

site.[19–26] This model produces expressions which allow resonant scattering of phonons and hence depressions in the conductivity curves. Expressions for scattering from a defect model consisting of a change of mass and a change of force constant to the six nearest neighbors have also given rise to the possibility of resonant scattering.[27–30]

This paper has four objectives: (1) to present experimental data on the thermal conductivity of sodium chloride containing the nine substitutional impurities, (2) to extend the validity of the usual Debye approximations by calculating phonon data for 64 000 points in the Brillouin zone and hence finding the density of states and group velocities, and (3) to use the phonon data to evaluate the expressions derived in Ref. 28 for isotope and substitutional defect relaxation rates. The model assumed for the defects is that of a mass change and simple force-constant change. (4) The fourth objective then is to see how well this model and our method of computing the conductivity can explain the experimental data.

Section II of this paper describes the experimental aspects of measuring the thermal conductivity of the nine systems mentioned above over the temperature range 1.2 to 300°K. Expressions used to calculate the thermal conductivity are presented in Sec. III.

Section IV describes our calculations of the density of states and frequency-averaged group velocities for NaCl using the shell model for the lattice. These are used to relax the Debye approximation.

Relaxation rates, based on expressions derived in Ref. 28, are given in Sec. V for isotope scattering and in Sec. VI A for impurity scattering. The former is an exact calculation, i.e., as good as the phonons obtained with the shell model, and the latter is exact within a simple model of the defect and within the phonon data. Section V contains a fit to the pure curve.

Section VI B discusses the results of the defect calculations and a comparison with our experimental data.

II. EXPERIMENTAL ASPECTS

A. Technique

The thermal-conductivity apparatus used for these measurements is described in detail elsewhere.[31,32] Two

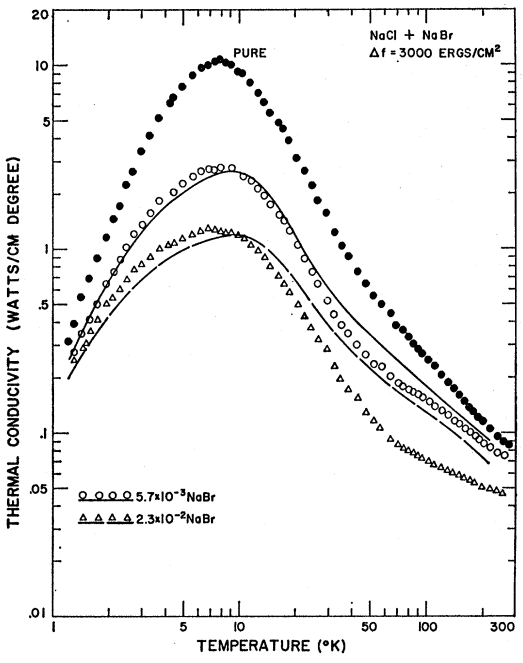

FIG. 2. Thermal conductivity of the system NaCl:NaBr. Points are the experimental data and the lines are the theoretical fits.

[19] S. Takeno, Progr. Theoret. Phys. (Kyoto) **29**, 191 (1963); **30**, 144 (1963).
[20] J. Callaway, Nuovo Cimento **29**, 883 (1963); J. Math. Phys. **5**, 783 (1964).
[21] J. Krumhansl, in *Proceedings of the 1963 International Conference on Lattice Dynamics* (Pergamon Press, Ltd., London, 1964).
[22] R. J. Elliott and D. W. Taylor, Proc. Phys. Soc. (London) **83**, 189 (1964).
[23] C. W. McCombie and J. Slater, Proc. Phys. Soc. (London) **84**, 499 (1964).
[24] A. A. Maradudin, Westinghouse Research Laboratory Report No. 64-929-100-P4, 1964 (unpublished).
[25] K. Thoma and W. Ludwig, Phys. Status Solidi **8**, 487 (1965).
[26] L. Gunther, Phys. Rev. **138**, A1997 (1965).
[27] M. V. Klein, Phys. Rev. **131**, 1500 (1963).
[28] M. V. Klein, Phys. Rev. **141**, 716 (1966).
[29] M. Yussouff and J. Mahanty, Proc. Phys. Soc. (London) **85**, 1223 (1965); **87**, 689 (1966).
[30] G. Benedek and G. F. Nardelli, Phys. Rev. **155**, 1004 (1967).
[31] M. V. Klein and R. F. Caldwell, Rev. Sci. Instr. **37**, 1291 (1966).
[32] R. F. Caldwell, Ph.D. dissertation, University of Illinois, 1966 (unpublished).

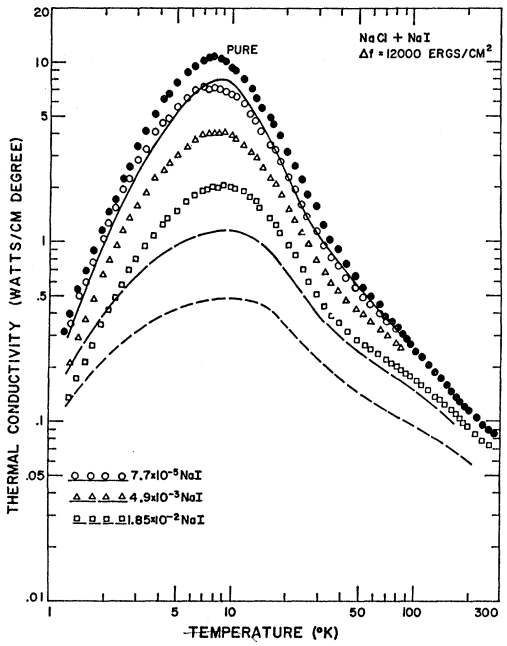

FIG. 3. Thermal conductivity of the system NaCl:NaI. Points are the experimental data and the lines are the theoretical fits.

cryostats were used to cover the entire temperature range. From 1.2 to 80°K a liquid-helium cryostat was used. Germanium resistance thermometers were used over this range. These had been previously calibrated against a vapor-pressure thermometer and a helium gas thermometer. The temperature range from 65 to 300°K was covered in a liquid-nitrogen cryostat which used platinum resistance thermometers. No corrections were made for radiation losses; so the data beyond 250°K are unreliable.

All of the crystals were grown by the Czochralski technique in an atmosphere of pure argon. Prior to the growing phase of the crystal preparation the sodium chloride starting material (reagent-grade powder from Mallinckrodt) was treated by passing Cl_2 gas through the molten salt for 12 h.

The analysis of the resultant boules was of two kinds. First, an analysis was made by running an ultraviolet absorption scan from 500 to 175 mμ on a Cary model 15 Spectrophotometer. This was done for three reasons: (a) to determine if any OH^- remained in the crystal after the Cl_2 treatment (OH^- band at 185 mμ), (b) to determine the relative concentrations between successive dopings of Ag^+, Tl^+, Li^+, Cu^+, and I^-, all of which have a uv band or bands, and (c) to determine if any of the uv active elements were contaminating the crystal.

The second analysis was quantitative. Commercial firms determined the F^- and Br^- concentrations by wet chemistry techniques and the Li^+, K^+, and Rb^+ concentrations by flame spectroscopy.

The NaI system was analyzed by two independent methods by the analytic staff within our Physics Department. The first determination was made by adding PdCl to an aqueous solution of the NaCl-NaI to form a colored solution of PdI which was then compared to a standard. The second method was to oxidize the I^- by adding HNO_3 dissolved in CCl_4 and then measure the absorption of violet light in the solution. The two methods yielded results that were within 10% of each other on the lightly doped sample, 6% on the medium-doped sample, and 2% on the heavily doped sample.

The concentrations of the impurities Ag^+, Tl^+, and Cu^+ were determined by the analytical staff within the Materials Research Laboratory. The silver concentration was determined by a gravimetric analysis and the copper by emission spectrographic analysis.

The thallium analysis was performed by Mossotti and Duggan of this laboratory by a calorimetric technique using Rhodamine B after a preliminary separation of the thallium from the sodium. The result of several independent determinations gave a ratio of 0.19 ± 0.02 ppm/cm^{-1} for the mole fraction TlCl/NaCl divided by peak-absorption coefficient in the uv absorption band at 200 mμ. We were able to grow only about 5 ppm mole fraction Tl^+ into our crystals. Because of its high vapor pressure, the thallium concentration in the melt, and hence in the boule, *decreased* during growth.

B. Results

The thermal-conductivity data are shown in Figs. 1–9 for the nine systems studied. The points show experimental data and the solid and dashed curves are the theoretical fits which are discussed in Sec. VI. The results of the concentration analysis are shown on each graph.

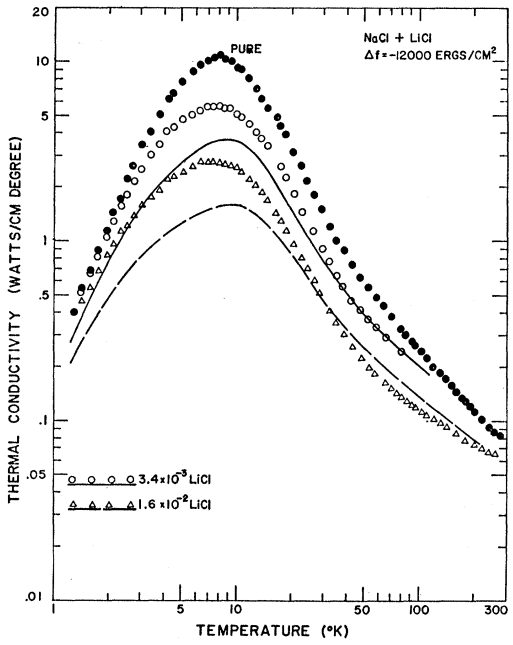

FIG. 4. Thermal conductivity of the system NaCl:LiCl. Points are the experimental data and the lines are the theoretical fits.

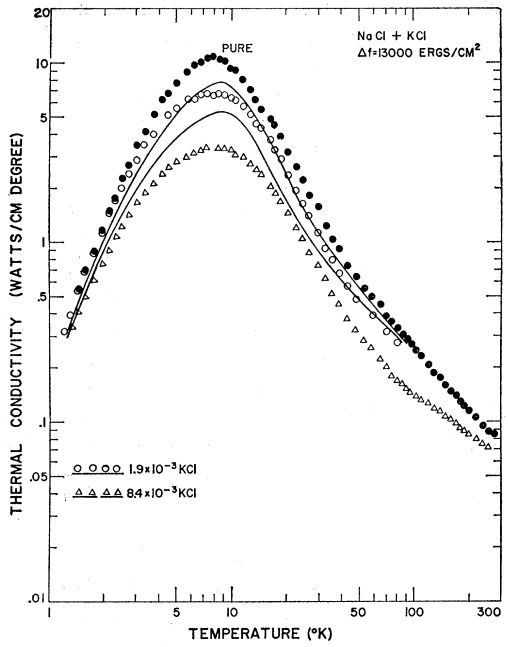

FIG. 5. Thermal conductivity of the system NaCl:KCl. Points are the experimental data and the lines are the theoretical fits.

One of the features to be noted about these curves is that with the possible exception of rubidium, they all exhibit non-Rayleigh scattering behavior. The deviation from Rayleigh scattering, which produces a symmetric lowering of the curve about the peak, is most pronounced in the Ag^+, Cu^+, and Br^- systems at the high temperatures and the F^- system at the low temperatures.

No theoretical analysis was done on the rubidium samples since not enough impurity could be grown into the crystal to make an appreciable effect on the conductivity. The one curve shown was grown from a melt containing over 1 mole% RbCl. Both the thallium and copper samples contained less impurity but they affected the conductivity, so an analysis was done on these systems.

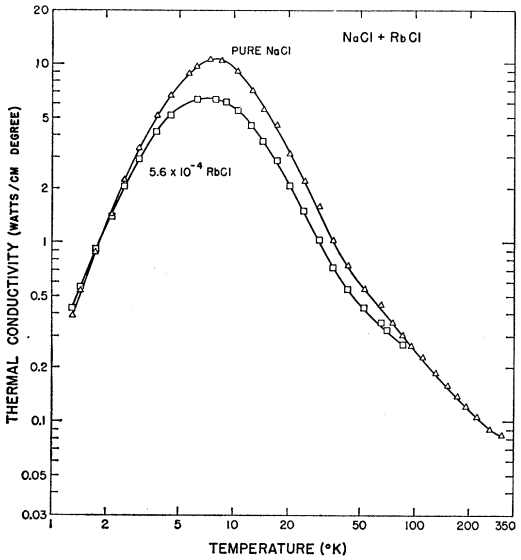

FIG. 6. Thermal conductivity of the system NaCl:RbCl. Experimental data only.

The following section gives the conductivity integral. Section IV describes our calculations giving us a detailed knowledge of the phonon spectrum so that the Debye approximation can be relaxed. The next step beyond this, i.e., the calculation of relaxation rates which are also valid outside the long wavelength and Debye approximations, is described in Secs. V and VI for the isotope and substitutional impurity rates, respectively.

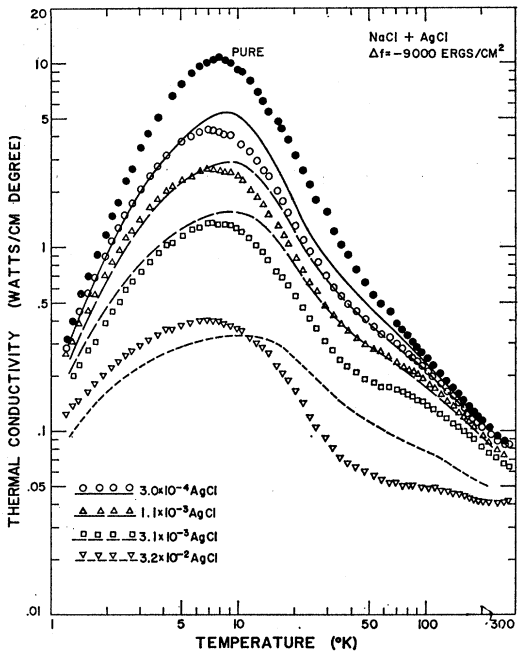

FIG. 7. Thermal conductivity of the system NaCl:AgCl. Points are the experimental data and the lines are the theoretical fits.

III. THE CONDUCTIVITY INTEGRAL

We shall use the following expression for the thermal conductivity:

$$K=(\hbar^2/3k_BT^2)\int_0^{\omega_m} d\omega[\langle\tau_c^{-1}\rangle]^{-1}\omega^2\langle|v|\rangle^2 \times\rho(\omega)e^x/(e^x-1)^2, \quad (1)$$

where

$$\tau_c^{-1}=\sum_i \tau_i^{-1} \quad (2)$$

is the combined relaxation rate due to several possible phonon-scattering mechanisms. $\rho(\omega)$ is the density of states, and the brackets $\langle\ \rangle$ indicate frequency averages.[33] The factor ω_m is the maximum frequency in the

[33] The proper average to take is $\langle\tau_c v_q^2\rangle$, but since $1/\tau_q$ (three phonon) is so poorly known it is felt that the averaging procedure used in Eq. (3) is entirely adequate and makes much more efficient use of computer time.

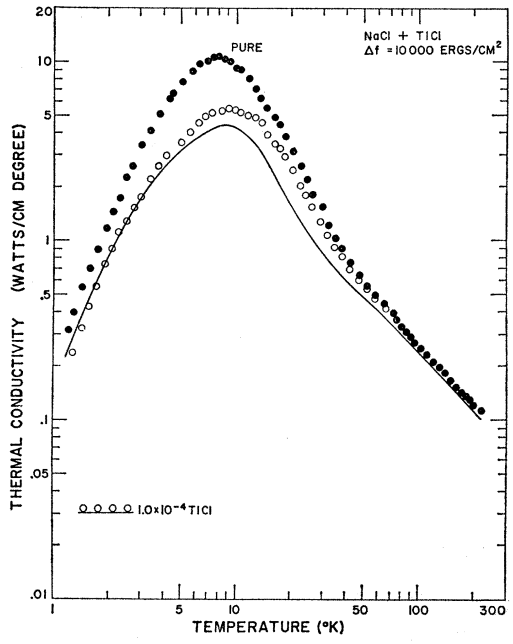

FIG. 8. Thermal conductivity of the system NaCl:TlCl. Points are the experimental data for a concentration of 5 ppm and the line is the theoretical fit for a concentration of 100 ppm.

lattice.[34] The next section is devoted to calculating $\langle|v|\rangle$ and $\rho(\omega)$. Discussion of the term $\langle\tau_c^{-1}\rangle$ will be delayed until Sec. V.

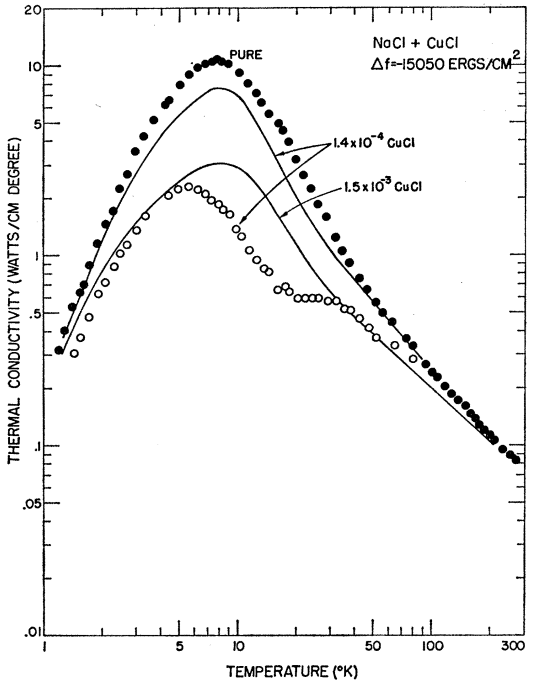

FIG. 9. Thermal conductivity of the system NaCl: CuCl. Points are the experimental data and the lines are the theoretical fits.

[34] Throughout this paper, ω denotes angular frequency in rad/sec.

TABLE I. Summary of input data for the shell-model-calculation parameters.

Elastic constants (10^{11} dyn/cm²):	$C_{11}=5.750$	$C_{12}=0.986$	$C_{44}=1.327$
Dielectric constants:	$\epsilon_0=5.45$	$\epsilon=2.349$	
Ionic polarizabilities (10^{-24} cm³):	$\alpha_+=0.255$	$\alpha_-=2.974$	
Reststrahlen frequency (10^{13} sec^{-1}):	$\omega_0=3.277$		
Lattice constant (10^{-8} cm):	$r_0=2.7935$		

IV. PHONON CALCULATIONS

Knowledge of the dispersion curves and polarization vectors of the individual phonons is necessary (a) to relax the Debye approximation by using more exact expressions for the phonon density of states and group velocities and (b) to calculate exact rates for phonon scattering by isotopes and substitutional impurities.

To obtain this detailed knowledge of the phonons, we have used the shell model that was successfully employed by Cochran *et al.*[35–37] at Chalk River to fit the neutron-determined phonon dispersion curves for KBr and NaI and more recently by Dolling *et al.*[38] to fit KI data.

Phonon frequencies and eigenvectors need only be computed for k vectors in 1/48 of the Brillouin zone; application of symmetry operations will then generate eigenvectors for points in the entire zone. The effect this has on expressions for densities of states is discussed in Appendix C of the paper by Timusk and Klein.[39] All calculations were performed on either the IBM 7094-1401 computer installation[40] or the "Illiac II"-1401 computer installation in the Department of Computer Science at the University of Illinois.

A. Determination of Input Parameters

There are nine parameters in this model[35–37]: A, B'', A', B', Z, α_+, α_-, d_+, and d_-. There exist, unfortunately, only five relations involving these nine parameters and the measurable constants listed in Table I. These are the same data used in similar calculations by Karo and Hardy[41] with the "deformation dipole" model. The elastic constants were obtained from data extrapolated to 0°K by Overton and Swim.[42] These relations are found in the Appendix of Ref. 35:

$$C_{11}=[e^2/(r_0v)][-2.555Z^2+(\tfrac{1}{2})(A+A'+B')], \quad (3a)$$

$$C_{12}=[e^2/(r_0v)][0.696Z^2-(\tfrac{1}{4})B'+(\tfrac{1}{4})A'-(\tfrac{1}{2})B''], \quad (3b)$$

$$C_{44}=[e^2/(r_0v)][0.696Z^2-(\tfrac{1}{4})B'+(\tfrac{1}{4})A'+(\tfrac{1}{2})B''], \quad (3c)$$

[35] A. D. B. Woods, W. Cochran, and B. N. Brockhouse, Phys. Rev. **119**, 980 (1960).
[36] A. D. B. Woods, B. N. Brockhouse, R. A. Cowley, and W. Cochran, Phys. Rev. **131**, 1025 (1963).
[37] R. A. Cowley, W. Cochran, B. N. Brockhouse, and A. D. B. Woods, Phys. Rev. **131**, 1030 (1963).
[38] G. Dolling, R. A. Cowley, C. Schittenhelm, and I. M. Thorsen, Phys. Rev. **147**, 577 (1966).
[39] T. Timusk and M. V. Klein, Phys. Rev. **141**, 664 (1966).
[40] The facility is partially supported by the National Science Foundation Grant No. NSF GP700.
[41] A. M. Karo and J. R. Hardy, Phys. Rev. **141**, A696 (1966).
[42] W. C. Overton and R. T. Swim, Phys. Rev. **84**, 758 (1951).

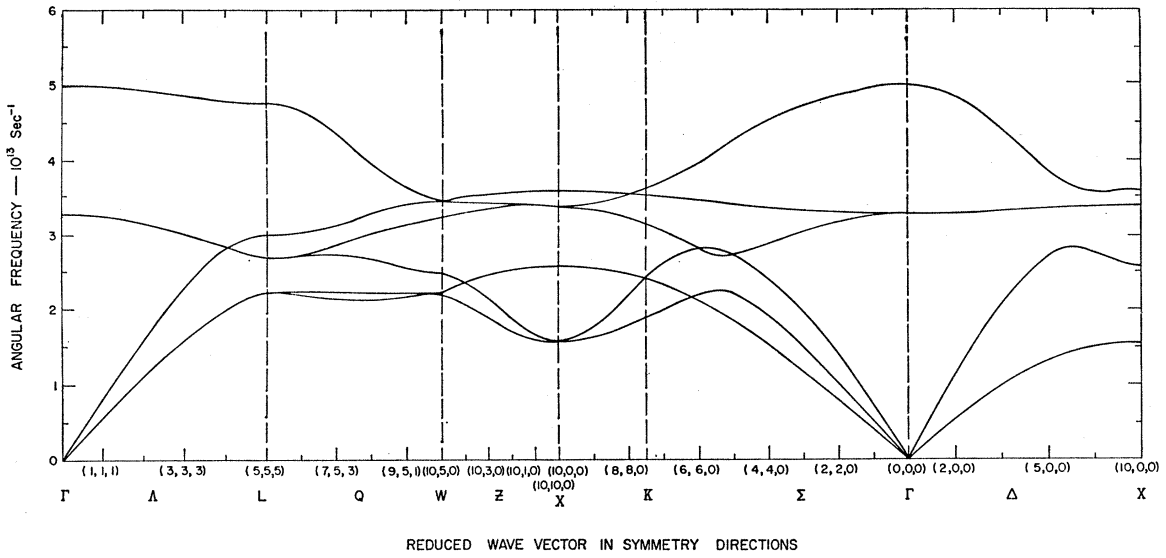

FIG. 10. Calculated dispersion curves for NaCl. Reduced wave vector is in units of $10\pi/r_0$.

$$\epsilon_0-\epsilon=4\pi(\epsilon+2)^2(Z+d_+-d_-)^2e^2/(9v\mu\omega_0^2), \tag{3d}$$

$$R_0=e^2[(d_+^2/\alpha_+)+(d_-^2/\alpha_-)]+\mu\omega_0^2[(\epsilon_0+2)/(\epsilon+2)]. \tag{3e}$$

The first three involve the elastic constants and the last two are the generalized Szigeti relations where μ is the reduced mass of the two ions and ω_0 is the TO phonon frequency at $k=0$.

Three of the parameters can be disposed of by making the not too unreasonable assumptions that the electronic polarizabilities are equal to the ionic polarizabilities listed in Table I and that the ionic charge $Z=1$. This leaves the five equations (3a)–(3e) for the remaining six unknowns. Two possibilities now present themselves for the sixth relation: (a) Assume a van der Waals force between next-nearest-neighbor ions, i.e., $V_2=a/r^6$, or (b) assume that the number of charges on each ion shell are equal, i.e., $Y_+=Y_-$.

Table II lists the results of using both of the assumptions. It is felt that the close agreement is somewhat fortuitous since Karo and Hardy used a Szigeti relation to obtain the parameter ϵ in Table I.

Since the van der Waals forces assumption seems more physically reasonable, it was used. The results in the form of dispersion curves in the various directions in k space are plotted in Fig. 10. A total of 64 000 points was used in the first Brillouin zone of k space.

B. The Density of States

The density-of-states histogram appearing in Fig. 11 was obtained by dividing the total frequency range into 75 bins. A second set of 75 bins over the entire range

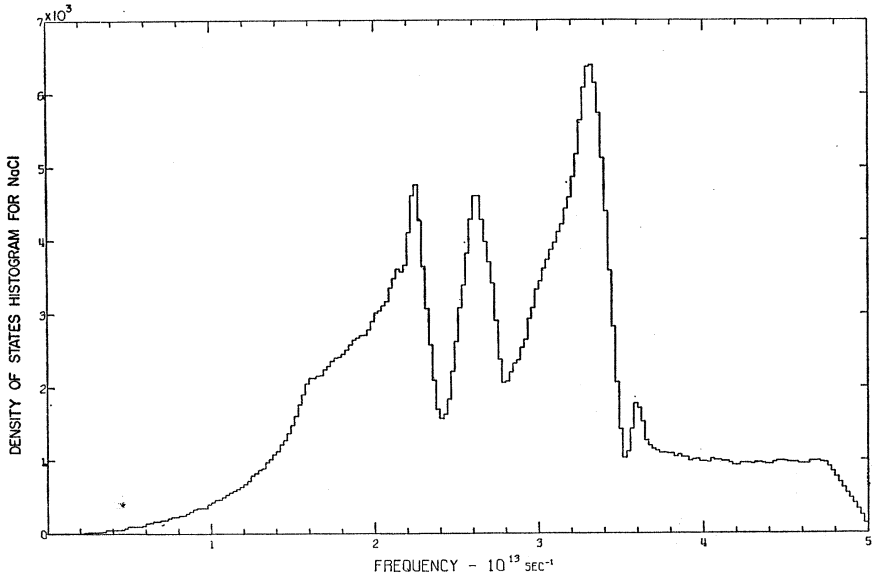

FIG. 11. Calculated density of states for NaCl for a total of 64 000×6 phonons.

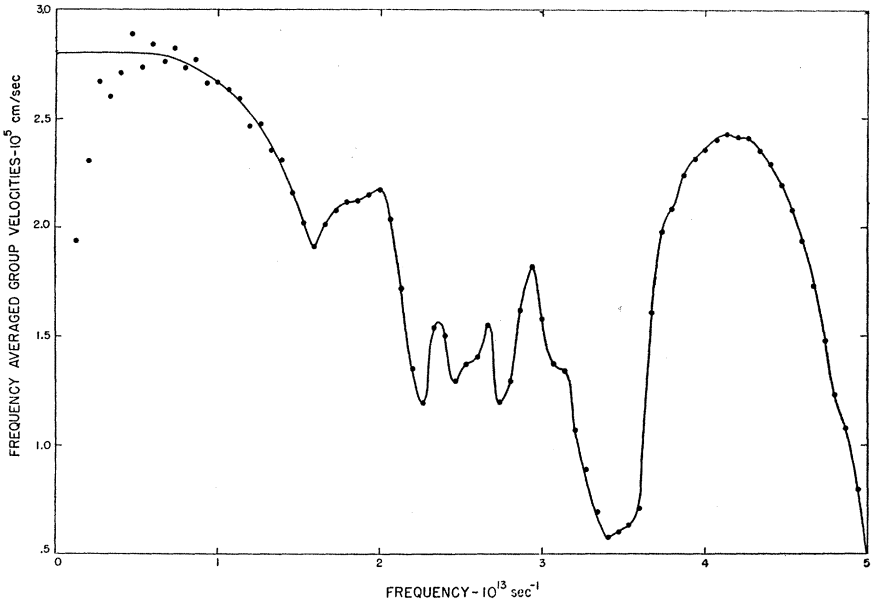

FIG. 12. Calculated group velocities for NaCl averaged over constant-frequency surfaces.

was defined so that the beginning of each bin was staggered with respect to the original set of bins a distance equal to $\frac{1}{3}$ a bin width to the left. A third set was similarly staggered $\frac{1}{3}$ a bin width to the right. The 225 sub-bins resulting from this staggering procedure were then averaged with proper care being taken at the ends to ensure that all of the points are counted within the original frequency span. The sum of the points under the histogram is $6\times64\,000=384\,000$.

C. Group Velocities

Figure 12 shows the average group velocity for the 64 000 phonons as a function of frequency. These were computed according to the equation

$$v_i(k\lambda)=\Delta\omega_i/\Delta k_i, \tag{4}$$

where i denotes one of the three Cartesian coordinates and $k\lambda$ denotes the phonon involved.

TABLE II. Shell-model-calculation parameters for two approximations.

Parameter	van der Waals forces	Equal charge
A	11.436	11.343
B''	0.180	0.180
A'	−0.294	−0.289
B'	0.042	0.040
Z	1.000	1.000
α_+ (10^{-24} cm^3)	0.255	0.255
d_+	0.023	0.024
α_- (10^{-24} cm^3)	2.974	2.974
d_-	0.280	0.281

V. ISOTOPE SCATTERING

A. Relaxation Rate

An exact expression for the relaxation rate due to phonon scattering by isotopes has been derived in Ref. 28. This expression was evaluated on the computer. Figure 13 shows the result of this calculation with the ω^4 dependence divided out or, in other words, shows the deviation from Rayleigh scattering. The three main peaks in the center correspond to the three main peaks of the density-of-states plot in Fig. 11. The general lowering of the curve at high frequencies reflects the fact that the heavier chlorine ion does not move as far from equilibrium as it does at low frequencies. At low frequencies the scattering rate is given by

$$1/\tau=3.00\times10^{-44}\omega^4\ \text{sec}^{-1}. \tag{5}$$

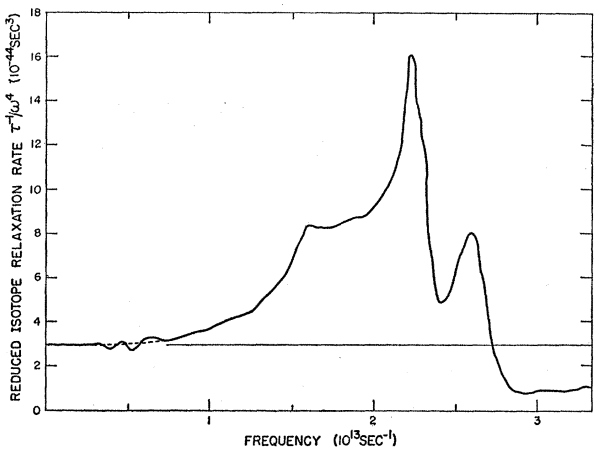

FIG. 13. Frequency-averaged relaxation rate divided by ω^4 for phonon scattering from chlorine isotopes in NaCl.

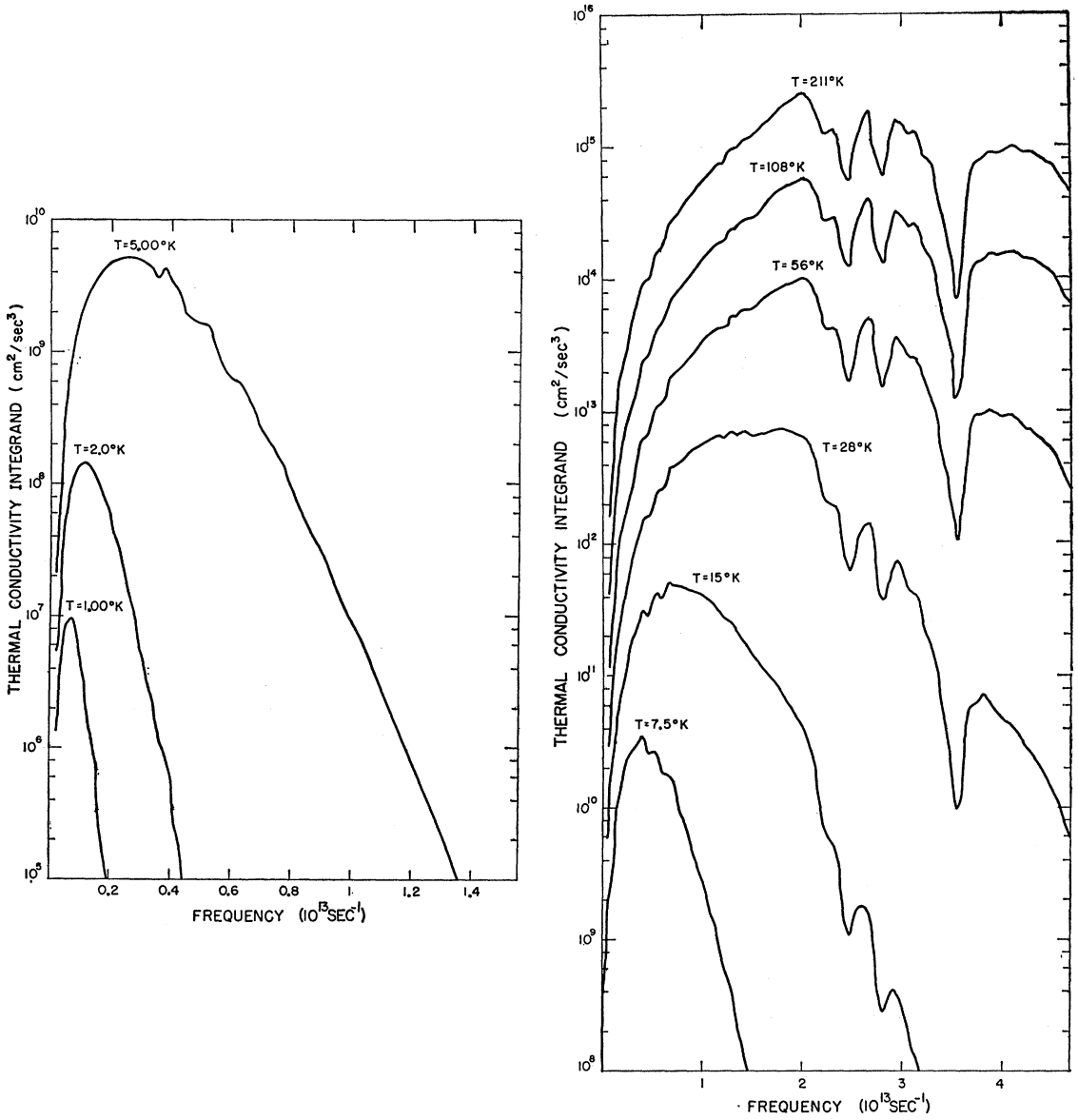

FIG. 14. Integrand of the thermal conductivity expression [Eq. (1)] without the factor $[\langle\tau_c^{-1}\rangle]^{-1}$: $\omega^2\langle|v|\rangle^2\rho(\omega)e^x/(e^x-1)^2$.

This is the same as would be obtained with Klemen's expressions[43] with the group velocity $v=2.93\times10^5$ cm/sec.

B. Fitting the Pure Curve

We are now in a position to relax the Debye approximation by using more realistic terms in Eqs. (1) and (2). The frequency-averaged group velocities $\langle v\rangle$ are shown in Fig. 12. The calculated density-of-states histogram $D(\omega)$ appearing in Fig. 11 is not the true density of states $\rho(\omega)$ but is proportional to it:

$$\rho(\omega)=1.58\times10^6 D(\omega). \quad (6)$$

[43] Reference 15, Eq. (45).

The factor $1/\tau_c$ in Eq. (1) contains four contributions for the pure crystal curve: (a) boundary scattering, (b) normal three-phonon processes, (c) umklapp three-phonon processes, and (d) isotope scattering. The isotope scattering term is shown in Fig. 13. The boundary scattering term was derived by Casimir, and for a crystal with a square cross section is

$$1/\tau\ (\text{boundary})=v/(1.12B), \quad (7)$$

where B should take on the value of the square root of the cross-sectional area, but for this calculation best results were obtained with $B=0.691\sqrt{\text{area}}$. This increase of $1/\tau$ above that predicted by Casimir seems to hold generally and is discussed in some detail by

Thatcher.[5] Klemens[44] has derived an expression for umklapp processes at low temperatures:

$$1/\tau \text{ (umklapp)} \propto e^{-\theta/aT}\omega^2T^3,$$

where $a\simeq 2$ for cubic crystals. Herring[45] has suggested that the normal process scattering rate should go as ω^2T^3 at low temperatures. For a good fit to our data at high temperatures the two three-phonon terms were condensed into one:

$$1/\tau \text{ (three phonon)} = 2.9\times10^{-18}e^{-50/T}\omega^2T \text{ sec}^{-1}. \quad (8)$$

The results are shown as the top solid line in Fig. 1. It is felt that the remaining deviation between this curve and the experimental data points is due, for the most part, to the poor expression for the three-phonon processes.

C. The Role of the Integrand and the Three-Phonon Processes

Before proceeding on to a discussion of the inclusion of defect scattering, it is profitable for us to look in more detail at the integrand of Eq. (1) without the τ_c factor and also at the three-phonon term given by Eq. (8).

Figure 14 shows that the integrand is a very sharply peaked function at low temperatures, e.g., at 1°K it falls off to 10^{-2} of its peak value in a frequency span of 0 to 0.2×10^{13} rad/sec. The effect of increasing the temperature is mainly to broaden the peak and shift it to higher frequencies. At 56°K, for instance, the main contribution (within a factor of 3) comes within the frequency span 1.0×10^{13} to 2.5×10^{13} rad/sec. Therefore, to have an appreciable effect on the conductivity at 55°K, the factor τ_c must have a large depression, or $1/\tau_c$ must have a large hump, within this range.

The combined relaxation rate $1/\tau_c$ is the sum of several terms, one of which is the three-phonon term shown for various temperatures as the solid lines in Fig. 15. Another one of the terms is the isotope term shown in Fig. 13 which reveals that it deviates from Rayleigh scattering most strongly in the region between 1.5×10^{13} and 2.5×10^{13} rad/sec. The dots on the three-phonon curves reproduce the isotope-relaxation rate of Fig. 13. The effect of the deviation from Rayleigh scattering on the conductivity curves will be washed out by the three-phonon processes at temperatures above 70°K. Below 30°K, however, the isotopes will dominate the three-phonon effects in this frequency range of 1.5 to 2.5×10^{13} rad/sec so that τ_c will be affected most by the isotopes at temperatures below 30°K. Between 30 and 70°K the isotope domination of $1/\tau_c$ is slowly replaced by three-phonon domination. Looking at the integrand curves of Fig. 14, we see that in the curve for $T=15$°K the major contribution to the integral occurs at frequencies less than 1.5×10^{13} rad/sec

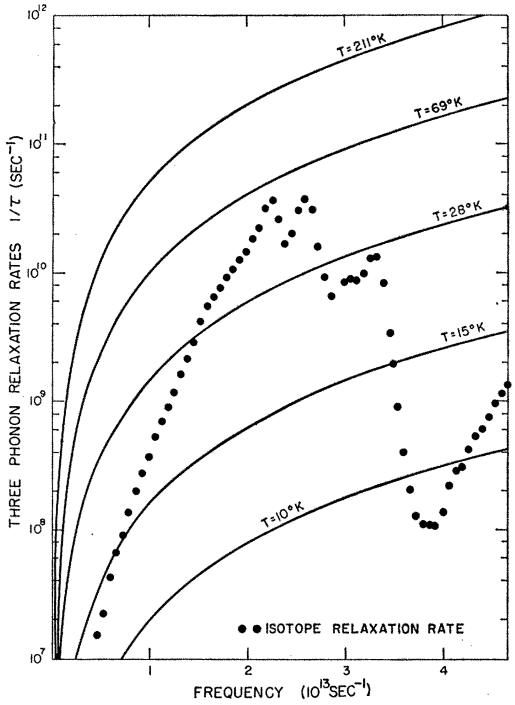

FIG. 15. Relaxation rates for the three-phonon processes [Eq. (14)] for various temperatures. The dots superimposed upon these form the curve for the isotope relaxation rate given in Fig. 13. This shows the various temperature-frequency combinations in which the isotope term will be important.

where the three-phonon effects still dominate. Thus we can say that the deviation from ω^4 Rayleigh scattering of phonons by isotopes, which is a reflection of the density of states, will make a contribution to the conductivity throughout the region between 20 and 70°K with the major effect being in the region 30–40°K.

VI. SCATTERING FROM SUBSTITUTIONAL IMPURITIES

A. Relaxation Rates

1. Introduction

Our model for the defect is a change of mass at the impurity site plus a change in central force constant to the six nearest neighbors.[28] With this model the perturbation matrix Γ is of order 9. By group-theoretical arguments this matrix can be reduced to a much simpler irreducible form, diagonal in one A_{1g} "breathing" configuration and two degenerate E_g "tetragonal" configurations, and having three identical 2×2 submatrices operating on two coupled odd T_{1u} configurations. The primed basis of Ref. 28 was used. Expressions for the scattering rate within each of these irreducible representations were derived in Ref. 28. We shall not reproduce them here but merely mention that they involve the imaginary part of the T matrix defined by

$$T=\Gamma[I/(I+G\Gamma)], \quad (9)$$

[44] P. G. Klemens, in *Encyclopedia of Physics*, edited by S. Flügge (Springer-Verlag, Berlin, 1956), Vol. 14, p. 198.
[45] C. Herring, Phys. Rev. **94**, 954 (1954).

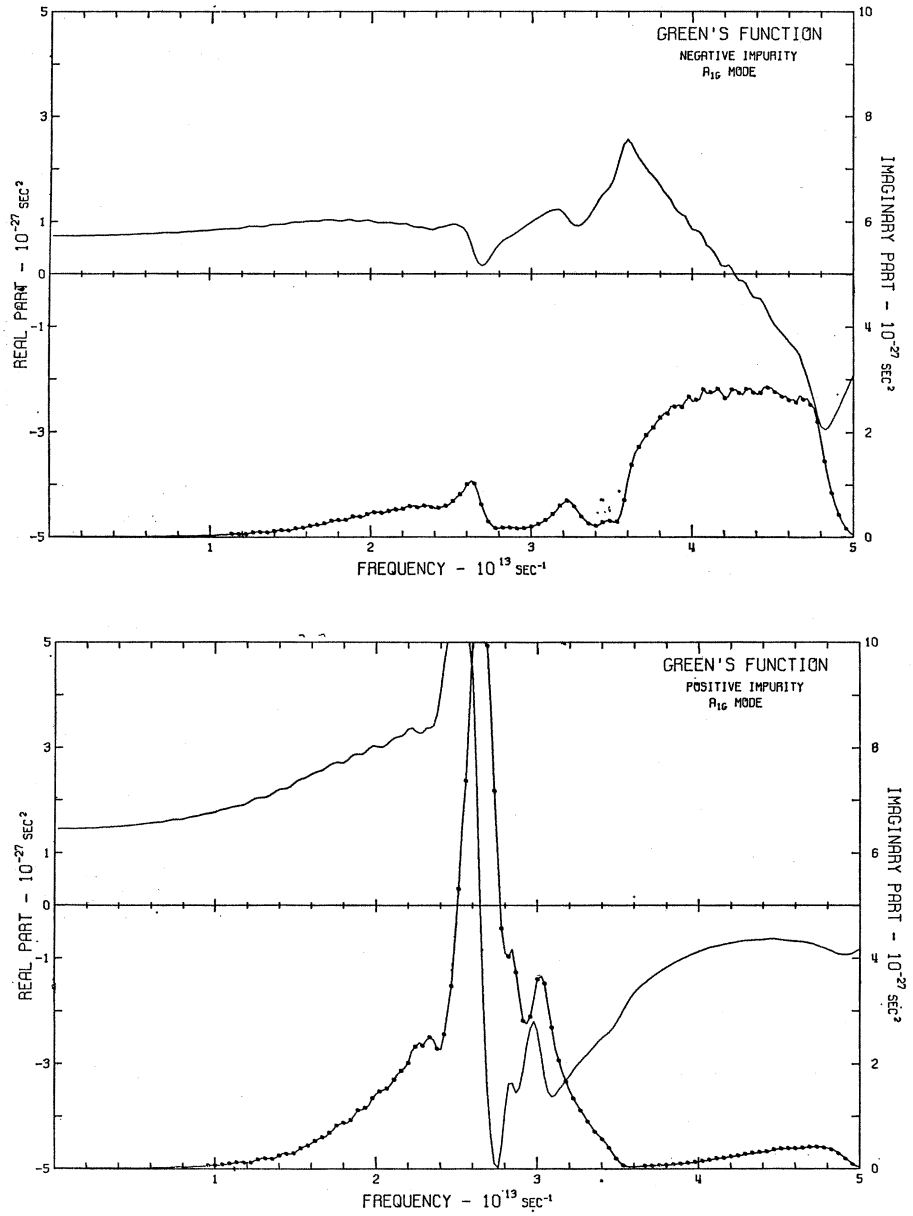

FIG. 16. Green's functions for the A_{1g} configuration in NaCl for both a positive- and negative-ion impurity. The real part is denoted by the smooth curve, the imaginary part by the curve with the dots.

where $\Gamma \equiv A' - A$ is the change in the dynamical matrix, and the Green's-function matrix G is given by

$$G \equiv [A - (\omega^2 + i\epsilon)I]^{-1}. \tag{10}$$

2. *Green's Functions*

In the basis spanned by the configurations just mentioned, G has the same number of components as the defect matrix Γ. Reference 39 gives the method used to calculate the real and imaginary parts of these matrix elements of G needed for the calculation of T and hence of τ_D. They are plotted in Figs. 16–20 for each of the five matrix elements for both a negative- and a positive-ion impurity. They were drawn on the basis of 225 frequencies, one in the center of each bin. There were originally 75 bins used to compute the histograms; they were then shifted over by plus or minus $\frac{1}{3}$ a bin width to provide a smoother and finer mesh. Nevertheless, we still had coarse graining effects, and the first 15 bins were forced to take the proper analytic frequency dependence. One can readily show that the imaginary parts in the long-wavelength limit must go as ω^3 for the A_{1g}, E_g, and T_{1u}-12 elements, ω^5 for the T_{1u}-22 elements, and ω for the T_{1u}-11 elements. Some small-scale wiggles can be seen in some of the curves because of residual coarse-graining effects.

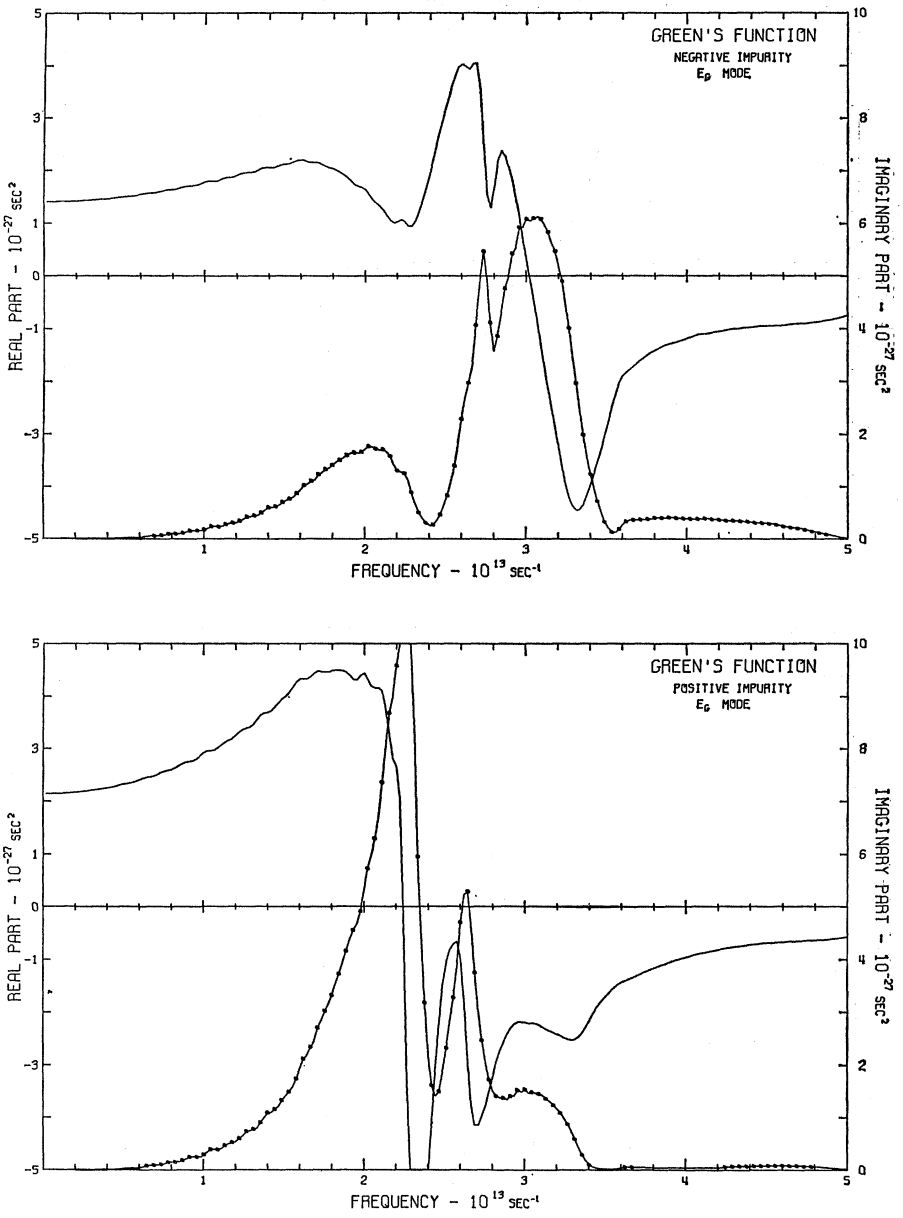

FIG. 17. Green's functions for the E_g configuration in NaCl for both a positive- and negative-ion impurity. The real part is denoted by the smooth curve, the imaginary part by the curve with the dots.

3. *Perturbation Matrix*

The expressions for the components of the perturbation matrix are given in Ref. 28 and are

$$\Gamma(A_{1g})=\Gamma_1(E_g)=\Gamma_2(E_g)=\Delta f/M_s, \quad (11a)$$

$$\Gamma_{22}(T_{1u})=\Delta f(2/M_i+1/M_s)-2RM_s\omega^2, \quad (11b)$$

$$\Gamma_{11}(T_{1u})=-RM_i\omega^2, \quad (11c)$$

$$\Gamma_{12}(T_{1u})=R(2M_iM_s)^{1/2}\omega^2, \quad (11d)$$

where $R=\Delta M_i/[M_i(M_i+2M_s)]$, M_i is the mass of the host ion at the impurity site, M_s is the mass of the nearest-neighbor ion, ΔM_i is the change of mass. Δf is the change in central force constant to the nearest neighbors, which we must now try to estimate.

4. *Theoretical Estimates of* Δf

When an impurity is added, the nearest neighbors will move to a new equilibrium position somewhere between that of sodium chloride and that of the dopant material. In order to calculate the change in nearest-neighbor force constant one must know what the new equilibrium position is.

Fukai has calculated[46] what these displacements should be by two different methods for the impurities

[46] Y. Fukai, J. Phys. Soc. Japan 18, 1413 (1963).

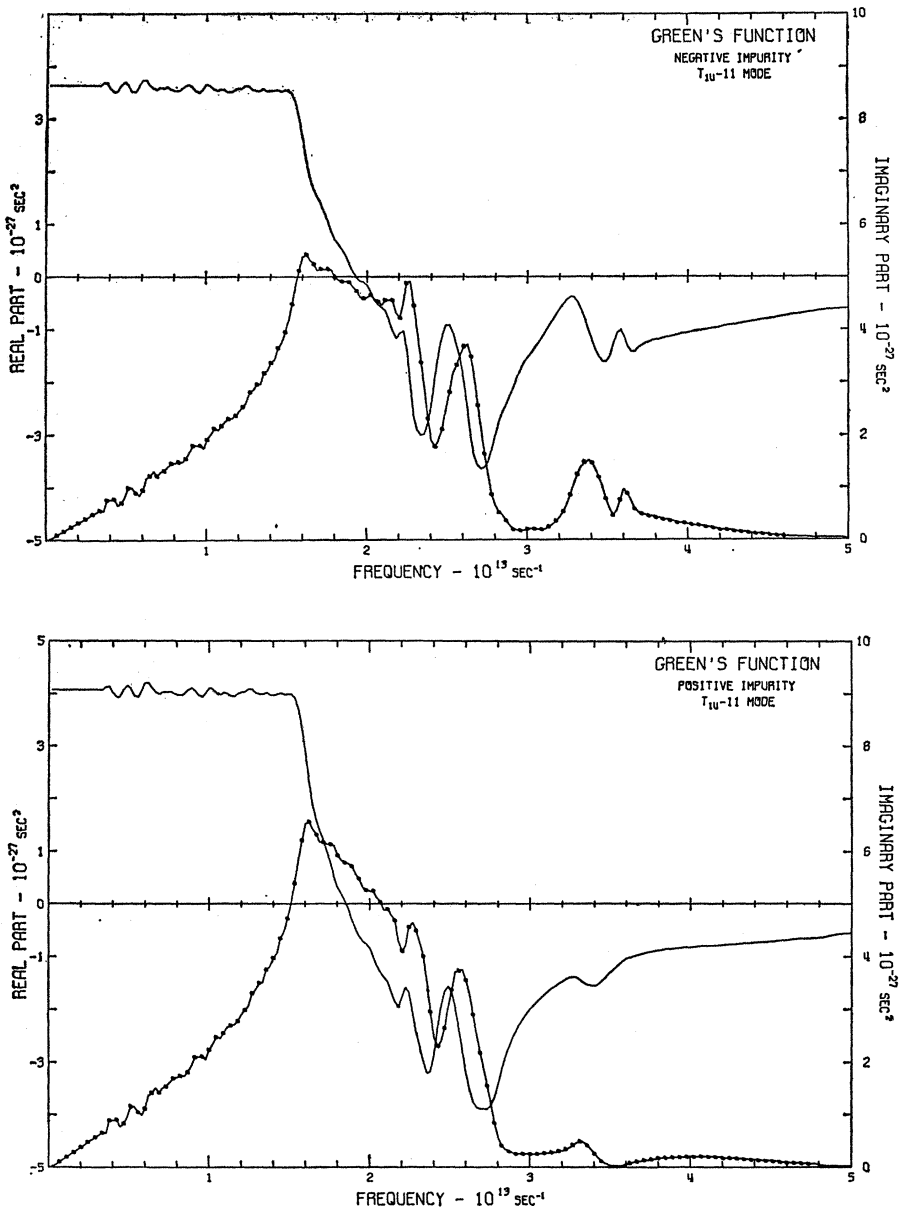

FIG. 18. Green's functions for the T_{1u}-11 configuration in NaCl for both a positive- and negative-ion impurity. The real part is denoted by the smooth curve, the imaginary part by the curve with the dots. The small scale wiggles are coarse-graining effects due to the finite mesh in k space.

F^-, Br^-, I^-, Li^+, K^+, and Rb^+ in NaCl. One method used the isotropic approximation of Brauer,[47] the other a discrete lattice-dynamical method due to Hardy,[48] which assumed the rigid-ion model for the phonons. Fukai has also experimentally measured the displacements for all the above impurities using nuclear-magnetic-resonance techniques.[49]

We now derive a method of determining these distances using the Green's function for the A_{1g} configuration at zero frequency. Although our derivation uses different language, the method is equivalent to that of Hardy.[48] The result that we shall obtain for the nearest-neighbor displacement u is contained in Eq. (15′) or (17) below.

The change in the force vector $\Delta F^{j\alpha}(L)$ along the bond lengths between the impurity and the nearest neighbors is in general given by

$$\Delta F^{j\alpha}(L)=-[(\partial V_i/\partial u^{j\alpha}(L))-(\partial V_0/\partial u^{j\alpha}(L))], \quad (12)$$

where u is the displacement from the old equilibrium position r_0. The subscript i denotes the bond between the impurity ion and the nearest neighbors and the subscript zero denotes the host bond. The remaining notation is that of Ref. 28. The first term on the right is evaluated at the new equilibrium position and the

[47] P. Brauer, Z. Naturforsch. **79**, 372 (1952).
[48] J. R. Hardy, J. Phys. Chem. Solids **15**, 39 (1960).
[49] Y. Fukai, J. Phys. Soc. Japan **18**, 1580 (1963).

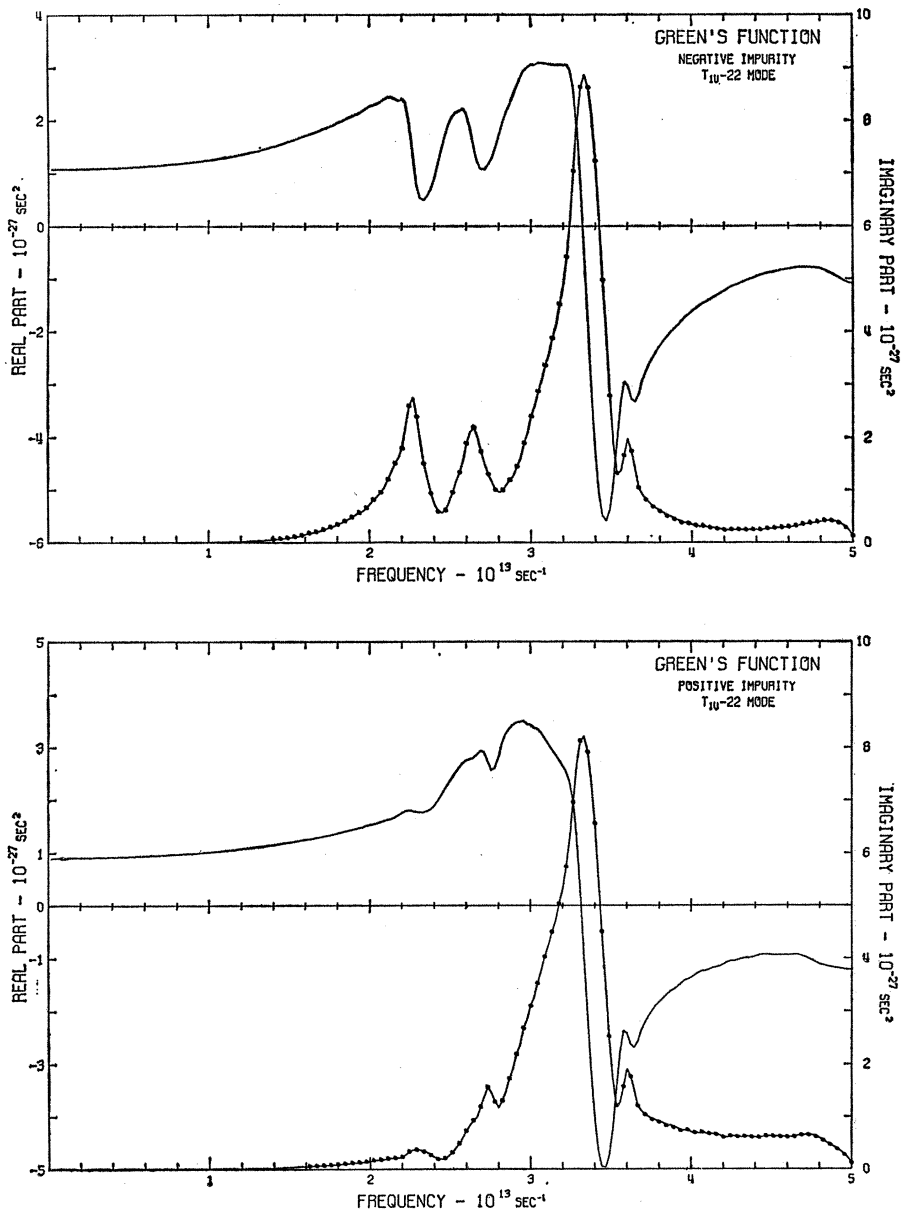

FIG. 19. Green's functions for the T_{1u}-22 configuration in NaCl for both a positive- and negative-ion impurity. The real part is denoted by the smooth curve, the imaginary part by the curve with the dots.

second is evaluated at the old equilibrium position. The vector $\Delta F^{j\alpha}(L)$ is localized and has A_{1g} symmetry. In fact we can write

$$\Delta F^{j\alpha}(L)=\Delta F e_{A1g}{}^{j\alpha}(L), \tag{13}$$

where $e_{A1g}{}^{j\alpha}(L)\equiv|A_{1g}\rangle$ is a unit vector of A_{1g} symmetry having components defined on the nearest-neighbor sites (having position vectors $\pm a\hat{\jmath}$; $\hat{\jmath}=\hat{1}, \hat{2}, \hat{3}$ are the unit vectors along the cube axes):

$$e_{A1g}{}^{j'\alpha}(\pm a\hat{\jmath})=\pm(1/\sqrt{6})(\delta_{jj'})$$

if α refers to nearest neighbors,

$=0$ at all other sites.

In Eq. (13) ΔF is given by

$$\Delta F=-[V_i'(r_0+u)-V_0'(r_0)], \tag{13'}$$

where the primes indicate derivatives with respect to r. Equation (13') is a scalar equation obtained by multiplying both sides of Eq. (13) by $e_{A1g}{}^{j\alpha}(L)$ and summing over L, j, and α, i.e., by taking the inner product with the vector $e_{A1g}{}^{j\alpha}(L)$.

The change $\Delta F^{j\alpha}(L)$ will be balanced by the (assumed) harmonic response of the rest of the lattice. At the new equilibrium position, the condition

$$0=\Delta F^{j\alpha}(L)$$
$$-[\sum_{L'}\sum_{\alpha'}\sum_{j'}\Phi^{jj'\alpha\alpha'}(L,L')u^{j'\alpha'}(L')-\text{correction}] \tag{14}$$

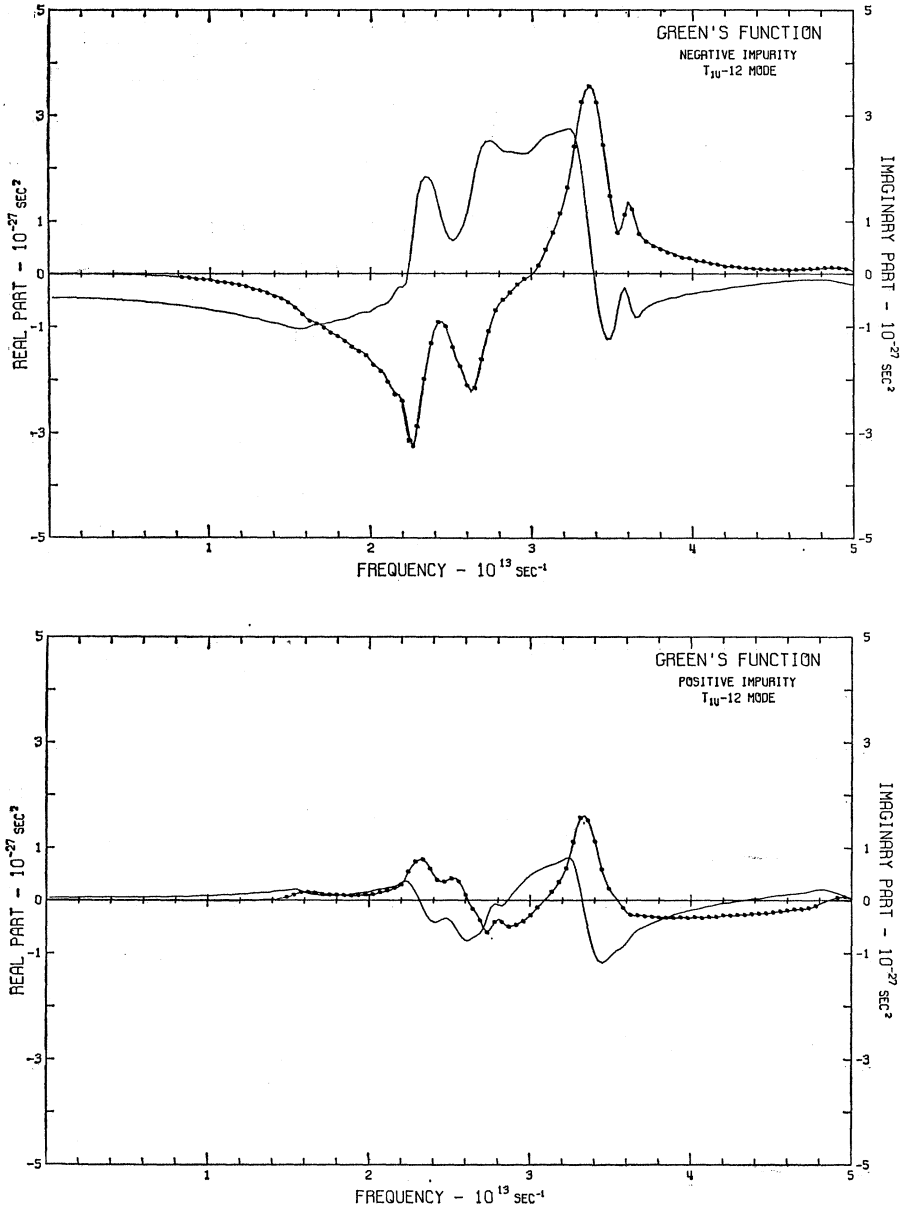

FIG. 20. Green's functions for the T_{1u}-12 configuration in NaCl for both a positive- and negative-ion impurity. The real part is denoted by the smooth curve, the imaginary part by the curve with the dots.

holds. The factor Φ is the unperturbed coupling constant matrix given in terms of the second derivative of the potential energy. The correction term comes from the fact that we have already taken care of the short-range force between the impurity and the nearest neighbors in Eq. (13). It can be written

$$\text{correction}=V_0''ue_{A1g}{}^{i\alpha}(L). \tag{14'}$$

Letting $\mathbf{\Phi}$ represent the matrix with components $\Phi^{ii'\alpha\alpha'}(L,L')$ and $\mathbf{u}$ the vector with components $u^{i\alpha}(L)$, we can use Eqs. (13) and (14') to write the formal solution of Eq. (14) as

$$\mathbf{u}=\mathbf{\Phi}^{-1}|A_{1g}\rangle(\Delta F+V_0''u).$$

We now take the inner product of this equation with $|A_{1g}\rangle$ and find that the displacement u of the nearest neighbors is given by

$$u=\langle A_{1g}|\mathbf{u}\rangle=\langle A_{1g}|\mathbf{\Phi}^{-1}|A_{1g}\rangle(\Delta F+V_0''u). \tag{15}$$

The matrix element of $\mathbf{\Phi}^{-1}$ appearing in Eq. (15) can be written

$$G_0(A_{1g})/M_s\equiv\langle A_{1g}|G(0)|A_{1g}\rangle/M_s.$$

Equation (15) can be written in the form used by Hardy,

$$u=\alpha F_r, \tag{15'}$$

where $F_r=\Delta F+V_0''u$ and $\alpha=G_0(A_{1g})/M_s$. The values

TABLE III. Summary of the nearest-neighbor equilibrium displacements and changes in force constant.

Impurity	Green's function u/r_0 %	Green's function Δf erg/cm²	Brauer u/r_0 %	Brauer Δf erg/cm²	Hardy u/r_0 %	Hardy Δf erg/cm²	Experimental u/r_0 %	Experimental Δf erg/cm²
F^-	−6.5	−18 500	−5.2	−19 000	−5.6	−18 000	−4.2	−19 000
Br^-	2.5	8800	4.1	2000	2.7	6800	5.5	−1600
I^-	6.2	14 900	9.5	2200	6.3	11 000	12.4	−5000
Li^+	−4.2	−10 600	−3.0	−13 000	−3.0	−13 000	−5.2	−8200
K^+	6.5	13 200	7.9	6600	5.3	16 000	9.2	2000
Rb^+	8.5	14 700	10.8	6500	7.5	19 000	9.8	9800
Ag^+	−1.2	15 800						
Tl^+	13.0	50 000						

for α that we obtained from our values of $G_0(A_{1g})$ were

$$\alpha_+ = 2.49\times10^{-5} \text{ cm/dyn for positive impurity,}$$
$$\alpha_- = 1.93\times10^{-5} \text{ cm/dyn for negative impurity.}$$

Hardy's value for α_+, obtained using a rigid-ion model[48] is $\alpha_+ = 2.04\times10^{-5}$ cm/dyne.

The short-range potential V is the only potential assumed to change when the impurity is added. It has the form

$$V = Ae^{-r/\rho}. \tag{16}$$

Thus the equilibrium condition, Eq. (15), becomes

$$(A_i/\rho_i)e^{-r_0/\rho_i}e^{-u/\rho_i} - (A_0/\rho_0)e^{-r_0/\rho_0} = [M_s/\mathrm{Re}G_0(A_{1g}) - (A_0/\rho_0^2)e^{-r_0/\rho_0}]u. \tag{17}$$

We have used Eq. (17) to obtain the values for the displacement u shown in the first column of Table III. In other columns we have listed the values found by Fukai using the Brauer method and the Hardy method plus the values obtained by Fukai from his nuclear-magnetic-resonance data. The input parameters used in our calculations were obtained from the following sources: The room-temperature values of the constants A and ρ were taken from Born and Huang[50] for all of the impurities except silver and thallium. For silver, the values of A and ρ were derived from the relations in Ref. 50, Eqs. (3.10)–(3.14), with the compressibility being obtained from elastic constant data given in Kittel[51] ($\beta = 2.26\times10^{-12}$ cm²/erg) and a van der Waals term given by Fukai[46] ($D/a^6 = 0.273\times10^{-12}$ erg). For thallium we obtained the compressibility from Tolpygo[52] ($\beta = 4.8\times10^{-12}$ cm²/erg) and the lattice constant from Kristofel[53] ($r_i = 3.38\times10^{-8}$ cm). A van der Waals term was not included, since it was unknown. Zero-degree values of r_0, ρ_0 for NaCl and of ρ_i for F^-, Br^-, I^-, Li^+, and K^+ were obtained from data tabulated by Karo and Hardy.[54] They also list 0° values for the compressibility and lattice constant, so that we were able to determine A_0 and A_i from the same relations in Ref. 50 as mentioned above. The values for u (and ΔF) that we obtained by the Green's-function method and show in Table III used the low-temperature parameters for these five impurities (F^-, Br^-, I^-, Li^+, and K^+). The values for other impurities that we obtained used the high-temperature parameters but, somewhat inconsistently, still used the value of the Green's function obtained with low-temperature phonons. Fukai used room-temperature parameters, exclusively.

An independent calculation of the displacements of the neighbors of Ag^+, Li^+, K^+, I^-, and Rb^+ in NaCl using the shell model has been made by Zhurkov and Oskot-skii.[55] Their results agree quite closely with those found by Fukai using the Hardy method for all of the impurities except Ag^+, which Fukai did not calculate. Their value for silver agrees quite well with that calculated by our Green's-function technique (Table III).

Once the new equilibrium displacement u is known, the change in force constant Δf can be calculated if a given force law is assumed. We have used a method due to Benedek and Nardelli.[30] They include the effective noncentral forces due to bond bending between nearest neighbors and handle the Coulomb part through the ionic polarizabilities:

$$2f = 2(\partial^2 V^R/\partial r^2) + 4(\partial V^R/r\partial r) - (e^*)^2(\alpha_+ + \alpha_-)/[D(\alpha_+ + \alpha_- + D)], \tag{18}$$

where $D = 6r^3/8\pi$, the derivatives are evaluated at the equilibrium distance, and e^* is the effective charge. f_0 is obtained by using the appropriate values for NaCl, and f_i is obtained by using the values of the impurity lattice and evaluating everything at the new equilibrium distance. Using this model we obtained $2f_0 = 30\,700$ ergs/cm² at room temperature and $2f_0 = 32\,800$ ergs/cm² at 0°K.

Another method of finding effective force constants, applicable to f_0, is to set f_0 equal to that value of $-\Delta f$ that will make the perturbed crystal unstable against a displacement in the $22(T_{1u})$ configuration, i.e., give a zero-frequency resonance. Using Eq. (22) we obtain

[50] M. Born and K. Huang, *Dynamical Theory of Crystal Lattices* (Clarendon Press, Oxford, England, 1954), p. 20.
[51] C. Kittel, *Introduction to Solid-State Physics* (John Wiley & Sons, Inc., New York, 1961), p. 63.
[52] K. B. Tolpygo, Izv. Akad. Nauk, SSR, Ser. Fiz. **24**, 177 (1960).
[53] N. N. Kristofel, Fiz. Tverd. Tela **3**, 1876 (1961) [English transl.: Soviet Phys.—Solid State **3**, 1366 (1961)].
[54] A. M. Karo and J. R. Hardy, Phys. Rev. **129**, 2024 (1963).
[55] I. S. Zhurkov and V. S. Oskot-skii, Zh. Eksperim. i Teor. Fiz. **43**, 2261 (1962) [English transl.: Soviet Phys.—JETP **16**, 1597 (1963)].

for a negative impurity

$$2f_0=\frac{2M_+M_-}{2M_++M_-}\Big/G_{22}^-(T_{1u})=30\,700\ \text{ergs/cm}^2, \quad (19)$$

and for a positive impurity

$$2f_0=\frac{2M_+M_-}{2M_-+M_+}\Big/G_{22}^+(T_{1u})=31\,500\ \text{ergs/cm}^2 \quad (20)$$

(at 0°K). The agreement with the results using Eq. (18) is not bad.

Table III summarizes our results for Δf. It was calculated using $\Delta f=(f_i-f_0)$. "Brauer" stands for Fukai's results using the Brauer method; "Hardy" his results using the Hardy method; and "Experimental" denotes his NMR results.

As will be discussed in the next section, the value entered here for silver is probably not correct. Even though the compressibility is smaller for AgCl than for NaCl, it apparently has a negative Δf. Its force-constant change, like that of copper, is calculated from optical data.

Because of the wide variety of values for Δf appearing here, they will be used merely as guide lines for the application of the theory to the experimental results. The seemingly unphysical negative results for Δf for Br^- and I^- as calculated from the experimental displacement serves to point out the futility of trying to obtain exact values for the change in force constant at the present level of experimental and theoretical knowledge.

5. *Expressions for the Relaxation Rates*

Since the relaxation rates for each mode q will go into an integral over ω, they should be converted to a frequency dependence. This is done by averaging the expressions for τ_D^{-1} in Ref. 28 over frequency. The results are

$$\langle 1/\tau(A_{1g})\rangle=(2cN\Delta\omega/\pi)\,\mathrm{Im}G(A_{1g})\times\mathrm{Im}T(A_{1g})/D(\omega), \quad (21a)$$

$$\langle 1/\tau(E_g)\rangle=(4cN\Delta\omega/\pi)\,\mathrm{Im}G(E_g)\times\mathrm{Im}T(E_g^1)/D(\omega), \quad (21b)$$

$$\langle 1/\tau(T_{1u})\rangle=(6cN\Delta\omega/\pi)\sum_{i,j}\mathrm{Im}G^{ij}(T_{1u})\times\mathrm{Im}T^{ij}(T_{1u})/D(\omega), \quad (21c)$$

where $D(\omega)$ is the calculated density-of-states histogram which appears in Fig. 11, and $\Delta\omega$ is the bin width.

The imaginary parts of T for the even configurations are given by the simple expressions

$$\mathrm{Im}T(A_{1g})=\frac{(\Delta f/M_s)^2\,\mathrm{Im}G(A_{1g})}{[1+\Delta f\,\mathrm{Re}G(A_{1g})/M_s]^2+[\Delta f\,\mathrm{Im}G(A_{1g})/M_s]^2}, \quad (22a)$$

$$\mathrm{Im}T(E_g)=\frac{(\Delta f/M_s)^2\,\mathrm{Im}G(E_g)}{[1+\Delta f\,\mathrm{Re}G(E_g)/M_s]^2+[\Delta f\,\mathrm{Im}G(E_g)/M_s]^2}, \quad (22b)$$

where M_s is the mass of the ions surrounding the impurity.

The odd configurations, being coupled, are not so easily treated. They involve three sets of 2×2 matrices which can then be separated into real and imaginary parts:

$$\mathrm{Im}T(T_{1u})=\mathrm{Im}\{\Gamma(T_{1u})[I+G(T_{1u})\Gamma(T_{1u})]^{-1}\}. \quad (22c)$$

This is easily done but the expressions get rather lengthy. They are obtained as follows:

When the 11, 22, and 12 elements of Eq. (22c) are written out and separated into their real and imaginary parts, they will all have the same denominator given by

$$\text{denominator}=[\det(I+G\Gamma)][\det(I+G\Gamma)]^*. \quad (23)$$

The real and imaginary parts of $\det(I+G\Gamma)$ are, in detail:

$$\mathrm{Re}\det(I+G\Gamma)=1+M_r\,\mathrm{Re}G_{22}\Delta f-(\mathrm{Re}G_{11}+M_p\,\mathrm{Re}G_{22}-2(\sqrt{M_p})\,\mathrm{Re}G_{12})(\Delta M/M_Q)\omega^2-[\mathrm{Re}G_{11}\,\mathrm{Re}G_{22}-\mathrm{Im}G_{11}\,\mathrm{Im}G_{22}-(\mathrm{Re}G_{12})^2+(\mathrm{Im}G_{12})^2]D_{FM}\omega^2, \quad (24a)$$

$$\mathrm{Im}\det(I+G\Gamma)=M_r(\mathrm{Im}G_{22})\Delta f-(\mathrm{Im}G_{11}+M_p\,\mathrm{Im}G_{22}-2(\sqrt{M_p})\,\mathrm{Im}G_{12})(\Delta M/M_Q)\omega^2-(\mathrm{Re}G_{11}\,\mathrm{Im}G_{22}+\mathrm{Re}G_{22}\,\mathrm{Im}G_{11}-2\,\mathrm{Im}G_{12}\,\mathrm{Re}G_{12})D_{FM}\omega^2, \quad (24b)$$

where $M_r=(M_i+2M_s)/M_iM_s$ is a reciprocal mass, $M_Q=M_i+2M_s$, $D_{FM}=\Delta f\Delta M/M_iM_s$, and $M_p=2M_s/M_i$; and, for instance, $G_{11}=G_{11}(T_{1u})$. The subscripts i and s indicate the *host* ion at the impurity and surrounding sites, respectively.

The numerators of Eq. (22c) are given in terms of Eqs. (24a) and (24b) by

$$\text{num-11}=[1+M_r(\mathrm{Re}G_{22})\Delta f](\Delta M/M_Q)\omega^2\ \mathrm{Im}\det(I+G\Gamma)-D_{FM}(\mathrm{Im}G_{22})\omega^2\ \mathrm{Re}\det(I+G\Gamma), \tag{25a}$$

$$\text{num-22}=[(M_p\Delta M/M_Q)\omega^2-M_r\Delta f+D_{FM}(\mathrm{Re}G_{11})\omega^2]\ \mathrm{Im}\det(I+G\Gamma)-D_{FM}(\mathrm{Im}G_{11})\omega^2\ \mathrm{Re}\det(I+G\Gamma), \tag{25b}$$

$$\text{num-12}=-[(\sqrt{M_p})\Delta M/M_Q+D_{FM}\ \mathrm{Re}G_{12}]\omega^2\ \mathrm{Im}\det(I+G\Gamma)+D_{FM}\ \mathrm{Im}G_{12}\omega^2\ \mathrm{Re}\det(I+G\Gamma). \tag{25c}$$

In the limit as $\omega\rightarrow 0$ the 11 contribution to $1/\tau$ will dominate for a system where ΔM is not zero. In this limit

$$\mathrm{Im}T^{11}(T_{1u})\rightarrow-(\Delta M/M_Q)^2(\mathrm{Im}G_{11})\omega^4. \tag{26}$$

The other two elements are considerably more complicated, but if we impose the two additional limits $\Delta f\rightarrow 0$ or $\Delta M\rightarrow 0$ we can get an idea of their behavior. In the limit $\Delta f\rightarrow 0$ and $\omega\rightarrow 0$, the denominator approaches unity and

$$\begin{aligned}\mathrm{Im}T^{22}(T_{1u})&\rightarrow-M_p(\Delta M/M_Q)^2(\mathrm{Im}G_{11})\omega^4,\\ \mathrm{Im}T^{12}(T_{1u})&\rightarrow M_p(\Delta M/M_Q)^2(\mathrm{Im}G_{11})\omega^4,\end{aligned} \tag{27}$$

and for $\Delta M\rightarrow 0$ and $\omega\rightarrow 0$ (but $\Delta f\neq 0$)

$$\begin{aligned}\mathrm{Im}T^{22}(T_{1u})&\rightarrow-M_r^2(\mathrm{Im}G_{22})(\Delta f)^2/[1+M_r(\mathrm{Re}G_{22})\Delta f]^2,\\ \mathrm{Im}T^{12}(T_{1u})&\rightarrow-(\Delta M/M_Q)(\mathrm{Im}G_{12})\Delta f\omega^2/[1+M_r(\mathrm{Re}G_{22})\Delta f].\end{aligned} \tag{28}$$

Thus we see that in all cases the imaginary part of the odd-parity T matrix goes as ω^5 in the long-wavelength limit. (Remember that $\mathrm{Im}G_{11}\rightarrow\omega$, $\mathrm{Im}G_{22}\rightarrow\omega^5$, and $\mathrm{Im}G_{12}\rightarrow\omega^3$.) In the expression for the relaxation rate, Eq. (21c), we see that these expressions get multiplied by the imaginary parts of the Green's functions and divided by the density of states, which goes as ω^2. Thus the (11) contribution will dominate when $\Delta M\neq 0$ and the relaxation rate goes as ω^4. In the extreme case of $\Delta M=0$ we see that the (22) element will dominate and the relaxation rate goes as ω^8 as discussed in Ref. 27.

From Eqs. (22a) and (22b) for the even-parity T matrices and Eqs. (21a) and (21b) for the even-parity contributions to the relaxation rate and the fact that $\mathrm{Im}G(\text{even})$ goes as ω^3 as $\omega\rightarrow 0$ we see that both even-parity contributions to the relaxation rates go as ω^4 in this limit also.

The nonperturbative character of the expressions for the relaxation rates can be seen by looking at the denominators of the T matrices. When perturbation theory holds, the denominators should be equal to unity. We will investigate this for the effect of a bromine impurity on the E_g configuration. A reasonable force-constant change from Table III would be 5000 ergs/cm^2 and Fig. 17 shows that at zero frequency $\mathrm{Re}G(E_g)=1.4\times10^{-27}$ sec^2 and $\mathrm{Im}G(E_g)=0$. Therefore

$$\text{Denom}=(1+5000\times1.4\times10^{-27}\times6.03\times10^{23}/23.0)^2=(1.18)^2.$$

This shows that even in the long-wavelength region perturbation theory would begin to break down for the force-constant change description.

Resonances, of course, will occur when the real part of these denominators goes to zero. This condition will be discussed more fully in the next section.

B. Sodium Chloride with Defects

1. General Remarks

In order to obtain the larger non-Rayleigh depressions of the conductivity curves due to the addition of defects which couple more strongly to the lattice, the same conditions mentioned above in Sec. V must hold. Within the "window" allowed by the integrand at the temperature of the depression, the defect-relaxation rate must have a contribution which will dominate those of all other processes, while at temperatures away from the depression the contribution will not be proportionally as large.

For low-temperature depressions, the three-phonon processes will be negligible, and all that is important is the large contribution within the peaks of the integrand. This will be within the frequency range of 0.1×10^{13} to 0.2×10^{13} rad/sec as shown in Fig. 14. For high-temperature depressions, on the other hand, the defect contribution to $1/\tau_c$ must occur within the range of 1.5×10^{13} to 2.5×10^{13} rad/sec allowed by the integrand at around 56°K and also must be the dominant term in $1/\tau_c$. A contribution as low as 1×10^{13} rad/sec would also contribute with the "56°K window," but it would give an even larger contribution at around 15°K which is not found experimentally.

The expressions for the frequency-averaged relaxation rates for the three configurations are given in Eqs. (21a), (21b), and (21c). Large contributions to these rates will appear when resonances occur in the T matrices of Eqs. (22a), (22b), and (22c).

An even-parity resonance will appear when

$$1+\Delta f\ \mathrm{Re}G/M_s=0. \tag{29}$$

At resonance the contribution to the average relaxation

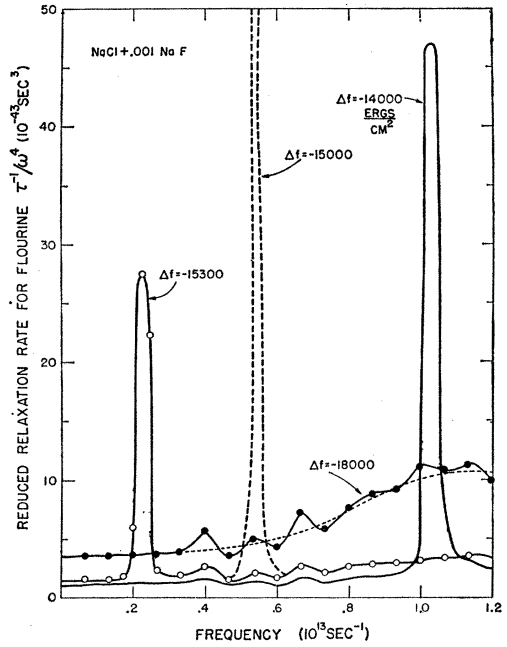

FIG. 21. Reduced relaxation rate for phonon scattering from fluorine impurity in NaCl for various force-constant changes. This is formed by dividing the total relaxation rate for an arbitrary concentration of 0.1 mole% by ω^4. The small wiggles in some of the curves are due to coarse-graining effects and are not real.

rate will be, from Eqs. (22a), and (22b),

$$\langle 1/\tau\rangle = 2cN\Delta\omega/\pi D(\omega) = 9.04\times 10^{15} c/D(\omega), \quad (30)$$

where again c is the fractional concentration of the impurity and N is the number of points in the Brillouin zone ($N=64\,000$). It is interesting to note that within the ideal "window" for a high-temperature depression ($1.5\times 10^{13}<\omega<2.5\times 10^{13}$ rad/sec), $D(\omega)$ from Fig. 11 has a minimum of 1.5×10^{3}. Therefore, with a typical concentration of 1×10^{-3} mole fraction the maximum value which Eq. (30) can attain is

$$\langle 1/\tau\rangle \cong 6\times 10^{9}\ \text{sec}^{-1}. \quad (31)$$

From Figs. 14 and 15 we see that in the temperature range in which this could be an important contribution to the integrand, the three-phonon processes dominate this value. Hence we must look elsewhere for the observed high-temperature depressions. Resonances in the even configurations might still contribute at low temperatures, however, since $D(\omega)$ at low frequencies is small.

An odd-mode resonance can occur when Re det given by Eq. (24a) is zero. Of particular interest is a resonance of this type which occurs when all but the first two terms are negligible, i.e., which

$$\text{Re det} \cong 1+M_r(\text{Re}G_{22})\Delta f. \quad (32)$$

This will always hold at low enough frequencies and is rigorous when $\Delta M=0$, $\Delta f\neq 0$. The 22-configuration corresponds to the impurity ion moving in a [100] direction, for example, with the two nearest-neighbor ions along that line moving out of phase with it, thus stretching two bonds. The reduced mass of the three ions undergoing this type of motion is $\mu=2/M_r$ so that the approximate resonant condition following from Eq. (32) is

$$1+2\Delta f\,\text{Re}G_{22}/\mu=0. \quad (33)$$

Looking at the low-frequency limit of Eqs. (25a), (25b), and (25c) we see that num-22 dominates and is given by

$$\text{num-22}\approx -M_r\Delta f\,\text{Im det}(I+G\Gamma). \quad (34)$$

From Eq. (24b) at low frequencies and near a "22 resonance" we obtain approximately

$$\text{Im det}\approx M_r\Delta f\,\text{Im}G_{22} +2[(\sqrt{M_p})/\Delta M/M_Q+(\text{Re}G_{12})D_{FM}](\text{Im}G_{12})\omega^2. \quad (35)$$

Both terms have the same limiting ω^5 frequency dependence. Thus, near a low-frequency "22-resonance" we have

$$\text{Im}T_{22}\approx -(M_r\Delta f)^2\,\text{Im}G_{22} \times\{[1+M_r(\text{Re}G_{22})\Delta f]^2+[M_r(\text{Im}G_{22})\Delta f +2((\sqrt{M_p})/\Delta M/M_Q+D_{FM}\,\text{Re}G_{12}) \times(\text{Im}G_{12})\omega^2]^2\}^{-1}. \quad (36)$$

We see, therefore, that in this approximation the occurrence of the resonance is due entirely to the force-constant change, independent of the mass change, but

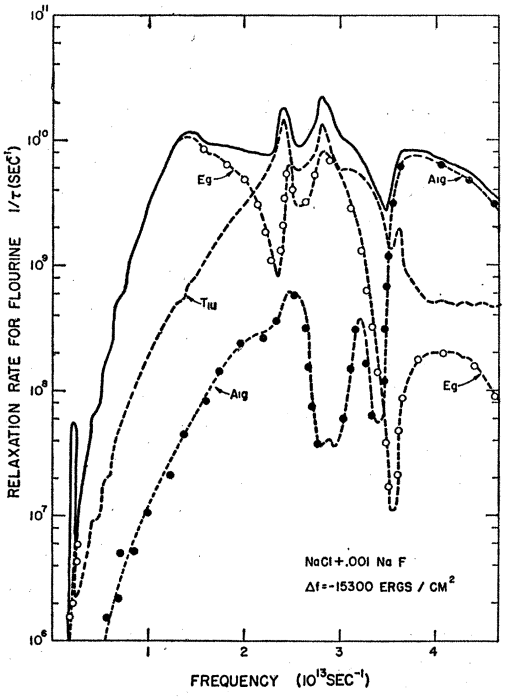

FIG. 22. Total relaxation rate for phonon scattering from fluorine impurity in NaCl for one force-constant change. Also shown are the contributions to the total from the E_g, A_{1g}, and T_{1u} configurations.

the width does depend on the change in mass as well as the change in force constant.

It should be emphasized that due to the smallness of $\mathrm{Im}G_{22}$ at low frequencies, the 22-element will dominate Eq. (21c) only at or very near the resonance. We now discuss our theoretical results for each impurity and how well they fit the experimental data.

2. *Fluorine*

We see from Fig. 1 that fluorine shows a large low-temperature depression. From the above discussion this could be explained by either an even-parity or an odd-parity configuration resonance. It turns out that the odd configurations give much better results. The odd-parity–configuration resonance condition discussed above, Eq. (32), applies here. Figure 21 shows the result of this odd-configuration resonance on the total reduced relaxation rate, which is formed by dividing the total relaxation rate for 0.1 mole% F^- given by the sum of Eqs. (21a), (21b), and (21c) by ω^4. With decreasing Δf, the resonance moves off to lower frequencies until it disappears completely when $\Delta f=-15\,350$ ergs/cm^2. Below the point where the resonant frequency is zero, the defect will resonate at a frequency which is imaginary, and hence the lattice will be unstable.[27]

Figure 22 gives the total relaxation rate for $\Delta f=-15\,300$ ergs/cm^2. This amounts to a total net force constant $f_0+\Delta f$ that is 0.3% of f_0, according to Eq. (19). This value of Δf gives a resonance at

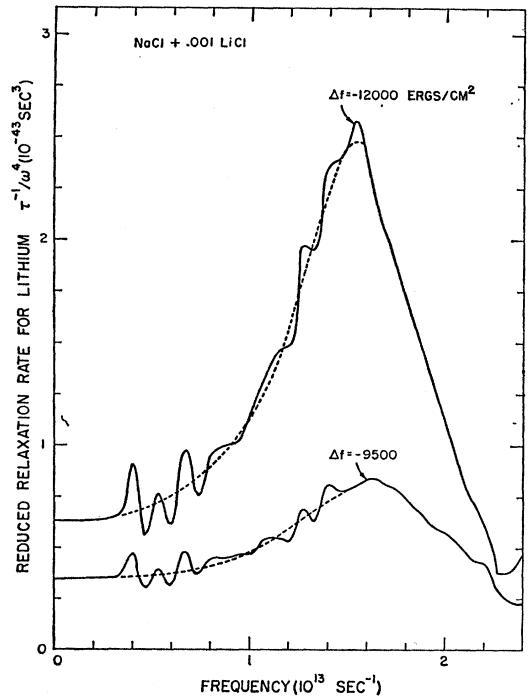

FIG. 23. Reduced relaxation rate for phonon scattering from lithium impurity in NaCl for various force-constant changes. The small wiggles are not real.

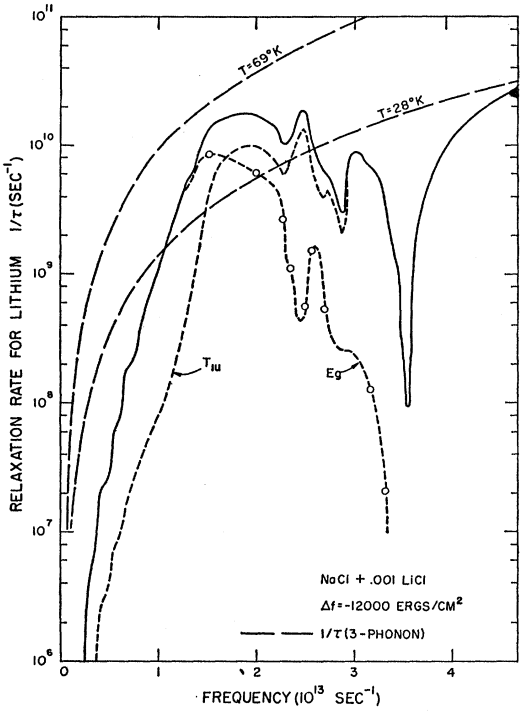

FIG. 24. Total relaxation rate for phonon scattering from lithium impurity in NaCl for one force-constant change. Also shown are contributions to the total from the E_g and T_{1u} configurations. The long dashed lines are the three-phonon rates from Fig. 15. They are drawn in to indicate when the defects will be important.

$\omega=0.2\times10^{13}$ rad/sec, which should give a far infrared absorption band at about 10 cm^{-1}. As mentioned above, this kind of resonance is due almost entirely to the change in force constant, and is essentially independent of the impurity mass. The plot in Fig. 22 and in all subsequent curves of this type is for a concentration of 0.1 mole%. The little spike at 0.2×10^{13} rad/sec in Fig. 22 will lie in the center of the integrand of Fig. 14 for $T=2$°K and will be well above the boundary-scattering term, $1/\tau(\text{boundary})=5\times10^5$ sec^{-1}. The contributions which the various configurations make to $1/\tau$ (defect) are also drawn in to indicate that for the most part either the even or the odd contributions dominate, so that we do not have to worry about the cross terms discussed in Ref. 28.

When we use this function for $1/\tau$ (defect) and add it to the other scattering rates and calculate the conductivity integral, we obtain the solid curves of Fig. 1. *The low-temperature depression does not show up in the theoretical curves despite the high peak at the proper frequency.* This must be caused by the extreme narrowness of the theoretical resonance peak, which means that although the phonons which are affected by the resonance are scattered quite strongly, the number of phonons involved is too small to make an appreciable contribution to the resistance. We conclude then that if this resonance is real, it must be broader than predicted to be effective in scattering phonons.

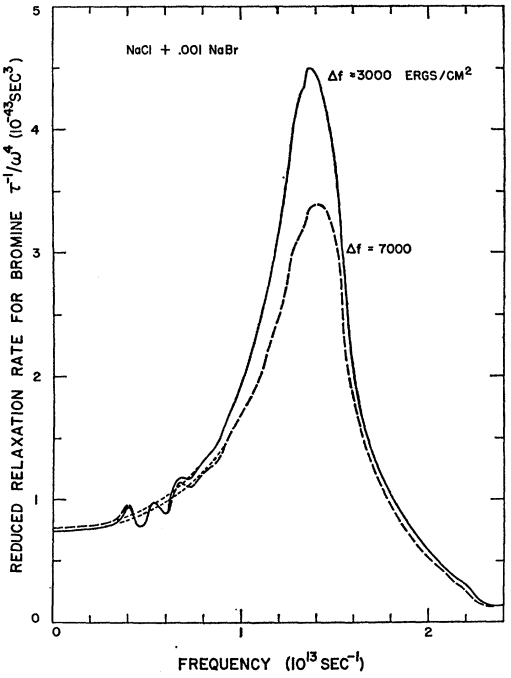

FIG. 25. Reduced relaxation rate for phonon scattering from bromine impurity in NaCl for various force-constant changes.

3. *Lithium*

The other ion investigated having a decrease in both the mass and force constant is lithium. The experimental depression in the conductivity is at about 50°K and is not too severe, so that what is needed is a broad, not too high, peak at around 2×10^{13} rad/sec. Table III gives values of the change in force constant lying between -8000 and $-13\,000$ ergs/cm^2. The plots of the reduced relaxation rates for two values of Δf within this range ($\Delta f=-9500$ and $-12\,000$) are given in Fig. 23. It should be noted that the theory *does* give a broad band at 1.6×10^{13} rad/sec for both of these values.

Figure 24 shows the over-all relaxation rate for a concentration of 0.1 mole% as well as the individual contributions of the different configurations. In addition, the long dashed lines give the value of the three-phonon processes for two temperatures. Two remarks can be made about this plot. The first is that for this concentration, the defect relaxation rate will at least be comparable to the three-phonon rate (and hence give a significant contribution to $1/\tau_c$) throughout the frequency range 1.2×10^{13} to 2×10^{13} rad/sec. From the integrand curves of Fig. 14 we see that this will have a considerable effect on the conductivity at around 28°K. The second remark is that the hump in $1/\tau$ (defect) comes from a combination of both the E_g and T_{1u} contributions. This indicates that the neglected cross term[28] between the even and odd modes might be important within this range, but this will not be pursued at this time.

To investigate the E_g contribution further we use the even-parity resonance condition of Eq. (29) with the value $\Delta f=-12\,000$ ergs/cm^2. For a resonance we would need $\mathrm{Re}G(E_g)=4.91\times10^{17}$ sec^2 which is near the value of 4.5×10^{-27} exhibited by $\mathrm{Re}G(E_g)$ in Fig. 17 at the peak frequency. Thus this peak is not a true resonance but a *near resonance*, and it occurs at $\omega=1.5\times10^{13}$ rad/sec and not at the center of the hump in the $\mathrm{Re}G(E_g)$ curve at 1.8×10^{13} rad/sec because the imaginary part of G becomes large on the high-frequency side.

Decreasing the change in force constant still further will, of course, make this hump more pronounced (a true resonance will occur at $-13\,000$ ergs/cm^2), but the only effect would be to increase the defect contribution at the lower temperatures where the contribution is already too large.

The odd-configuration contribution is due to a similar near resonance at $\omega=1.9\times10^{13}$ rad/sec and is in the 2-configuration. This type of near resonance is discussed in more detail below for the bromine and iodine systems.

The theoretical thermal-conductivity results are shown in Fig. 4 for $\Delta f=-12\,000$ ergs/cm^2. The high-temperature fit is quite good, but the curves are depressed too far near the maximum and on the low-temperature side. The biggest deviation occurs near 6° where the three-phonon rates are very small. In the

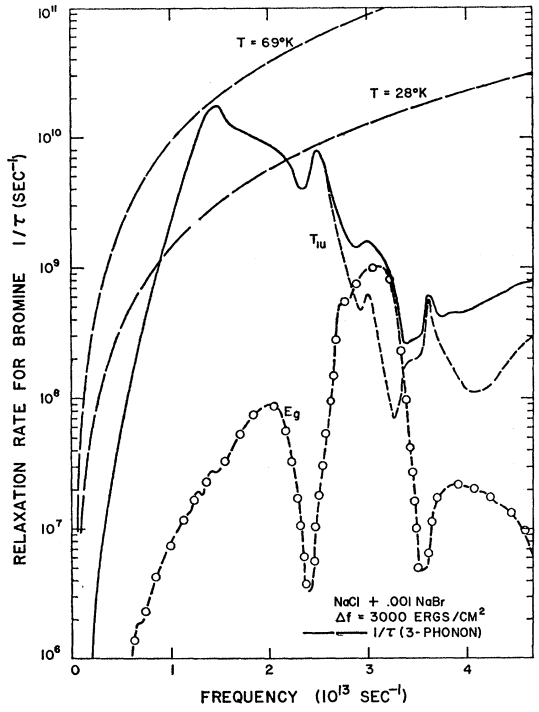

FIG. 26. Total relaxation rate for phonon scattering from bromine impurity in NaCl for one force-constant change. Also shown are the contributions to the total from the E_g and T_{1u} configurations. The long dashed lines are the three-phonon rates from Fig. 15. They are drawn in to indicate when the defects will be important.

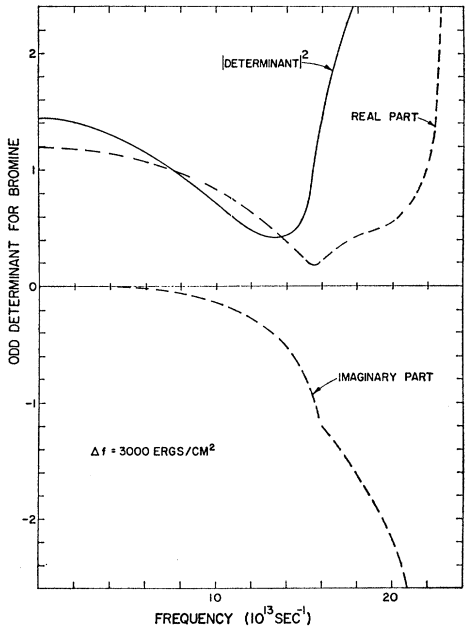

FIG. 27. Determinant of the 2×2 submatrix $(1+G\Gamma)$ within the odd configuration for a force-constant change of 3000 ergs/cm² and for a bromine impurity. This is an example of an incipient resonance since the real part does not reach zero but does have a distinct minimum.

frequency range of the "window" allowed by the integrand, Fig. 14, the theoretical defect-scattering rates are too large compared to those due to isotopes and to the boundary even though no hump occurs here. We do not know why.

4. *Bromine*

The impurities bromine and potassium are roughly twice as heavy as the host ion for which they substitute. Experimentally, both show a high-temperature conductivity depression with bromine being about twice as strong a scatterer as potassium. Figure 25 shows the plot of the reduced relaxation rates for bromine for a concentration of 0.1 mole%. The range of the change of force constant is given in Table III to be around 3000 to 7000 ergs/cm². From the figure we see that this change does have a small effect on the height and the width of the peak of $1/\tau$ but does not shift it appreciably from its position of 1.4×10^{13} rad/sec. The entire curve is higher than that for lithium, as we might hope from the experimental data. The peak also has its major contribution within the integrand curve for 28°K appearing in Fig. 14, but it is not as broad as the lithium peak. The relaxation rate for bromine, when compared in Fig. 26 with that for the three-phonon processes, shows that the peak $1/\tau$ (defect) will dominate the three-phonon processes at 28°K, so we again expect the major contribution from the Br^- to occur near this temperature.

This figure also shows that the odd configurations are by far the major contributors. The reason for this is shown in Fig. 27 where the real and imaginary parts of the odd determinant are plotted as the dashed lines. The solid curve is

$$|\det(I+G\Gamma)|^2=[\mathrm{Re}\det(I+G\Gamma)]^2+[\mathrm{Im}\det(I+G\Gamma)]^2. \quad (37)$$

Thus we see that although there is not a true resonance, we have again a near resonance at $\omega=1.3\times10^{13}$ rad/sec which will still give a peak in the relaxation rate. In this frequency range the 11 element of the T matrix is larger than but does not dominate the other elements of the odd-configuration submatrix. From Eq. (21c) and the fact that the imaginary part of G for the 11 elements dominates the other two elements, we have that the 11 elements dominate $\langle 1/\tau\rangle$.

The results, as shown in Fig. 2, give a reasonable fit at high temperatures, but the theoretical depression is not strong enough and it is centered more around 40°K whereas the experimental depression is nearer 60°K. The low-temperature fit is much better than that for lithium since, experimentally, bromine is a better scatterer in this region.

5. *Potassium*

Experimentally, potassium shows less high-temperature scattering than bromine and about the same as lithium. This is borne out by the total theoretical

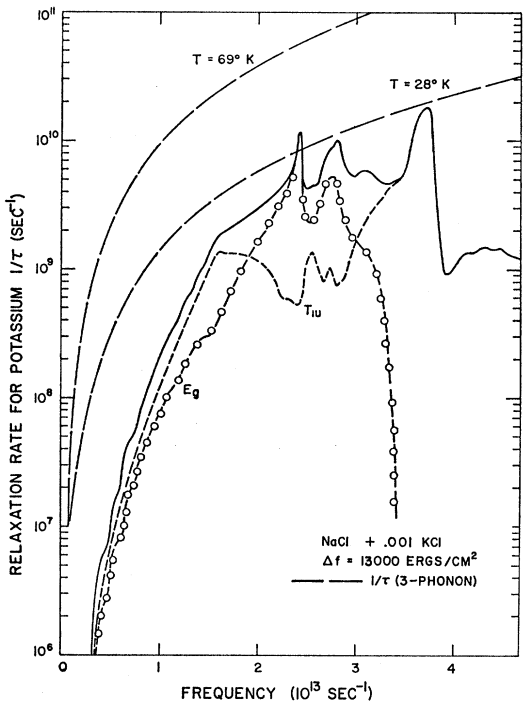

FIG. 28. Total relaxation rate for phonon scattering from potassium impurity in NaCl for one force-constant change. Also shown are the contributions to the total from the E_g and T_{1u} configurations. The long dashed lines are the three-phonon rates from Fig. 15. They are drawn in to indicate when the defects will be important.

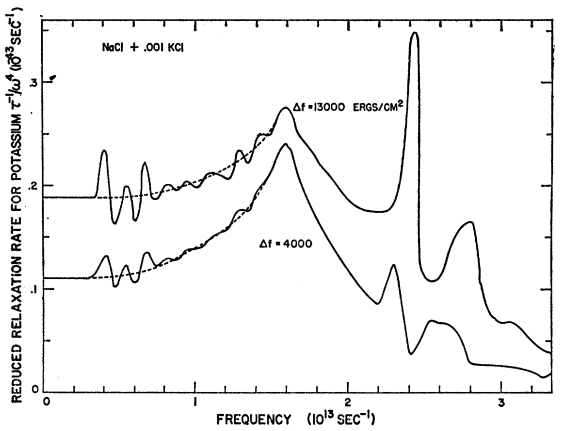

FIG. 29. Reduced relaxation rate for phonon scattering from potassium impurity in NaCl for various force-constant changes.

relaxation rate plotted in Fig. 28 for potassium. This uses a change of force constant equal to 13 000 ergs/cm² which is in the upper bracket of the values in Table III. The plot of the reduced relaxation rates for this value of Δf along with one for 4000 ergs/cm², which is in the lower limit of those appearing in Table III, appears in Fig. 29.

Even though the structure in these curves is small and will make only a token contribution to the resistivity, it is worth a little study. Discussing the two sharp E_g peaks at the higher frequencies first, we see from the resonance condition for even-parity configurations, Eq. (29),

$$\mathrm{Re}G(E_g) = -35.5\times1.66\times10^{-24}/13\,000 = -4.53\times10^{-27}\ \mathrm{sec}^2. \quad (38)$$

Laying this value out on the plot of $\mathrm{Re}G(E_g)$ in Fig. 17 we see that the first sharp peak at $\omega=2.4\times10^{13}$ rad/sec corresponds to a true resonance at a point where the imaginary part is near a minimum, and the second, broader peak, at $\omega=2.8\times10^{13}$ is a near resonance, also near an imaginary part minimum.

The broad odd-configuration peak at 1.6×10^{13} rad/sec is not due to a resonance, or even a near resonance, since the odd determinant is essentially flat throughout this region. The total denominator, not shown here, is 3.34 at zero frequency, 3.05 at $\omega=1\times10^{13}$ rad/sec, reaches a minimum of 2.90 in the frequency region from 1.3 to 1.5×10^{13} rad/sec, and then rises steadily to 5.77 at 2×10^{13} rad/sec. The peak in τ^{-1} is undoubtedly due to $\mathrm{Im}G_{11}(T_{1u})$ as shown in Fig. 18, which comes into the terms in the numerator as indicated in Eq. (26). The peak corresponds to the edge-of-zone Van Hove singularity for the ⟨100⟩ transverse acoustical phonons.

Figure 5 shows the result of this relaxation rate on the conductivity. Again there is a small depression on the high-temperature side, but it is not enough. This time it occurs at about 25°K and is due mainly to the small odd-parity hump. The three-phonon processes allow this to show up below 28°K; between this temperature and 15°K, the window allowed by the integrand is favorable, but the hump is not large enough.

6. *Iodine*

The ions Rb^+ and I^- are next in size, rubidium being about 3.5 times as heavy as Na^+ and I^- about 4 times as heavy as Cl^-. Unfortunately, not enough rubidium could be grown into the crystal to make any significant change in the conductivity, and so we shall discuss the analysis for I^- only.

Table III gives an average value of Δf for I^- to be around 12 000 ergs/cm². Calculations show that, as in the case of bromine, the odd configurations are predominant over the frequency range of interest, and again it is the 11 element that contributes most to $1/\tau$. The scattering rate at low frequencies is a little over 4 times as strong as for bromine, and the peak is about 5 times as strong as for bromine. The raising of the strength at low frequencies is exactly that expected from Eq. (26) since the ΔM's differ by a little over a factor of 2. [Equation (26) is only approximately correct in this frequency range.]

Figure 3 shows the resulting calculated conductivity curves. The predicted defect scattering will completely dominate the three-phonon effects for a broad range of frequencies at temperatures around 28°K. The result is the extremely large lowering of the conductivity curve

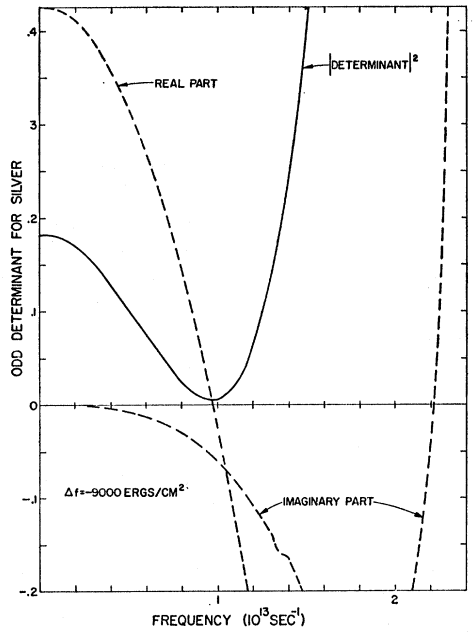

FIG. 30. Determinant of the 2×2 submatrix $(1+G\Gamma)$ within the odd configuration for a silver impurity in NaCl with a force-constant change of −9000 ergs/cm². This is an example of a sharp resonance, since the imaginary part is small at the point where the real part is zero.

shown in Fig. 3, which is not found experimentally. There is no reasonable value for Δf that will change this overestimate that the theory gives for the phonon-scattering rate of I^-.

7. Silver

The silver-ion impurity, despite the fact that it has a larger mass than sodium and the fact that the compressibility of AgCl is smaller than that of NaCl, apparently has a negative change in force constant when placed in NaCl. The increased value of $\Delta f = 15\,800$ ergs/cm^2 in Table III was derived using the lower value of compressibility. Evidence of a lowering of force constant in NaCl, however, comes from both the decrease in lattice constant of AgCl over NaCl and the optical data of Weber.[56] He found an infrared absorption at $52\ \text{cm}^{-1} = 0.98\times10^{13}$ rad/sec, which we can attribute to an odd-parity resonance. From Eq. (24a) for the real part of the determinant we calculate the change in force constant needed to give this resonance frequency to be $\Delta f = -9000$ ergs/cm^2. This is another example of the "22-resonance" discussed above in connection with the fluorine impurity.

The plot of the real and imaginary parts of the determinant and the entire denominator are shown in Fig. 30 for this resonance value of Δf. Figure 31 gives the reduced reciprocal relaxation rates for various force-constant changes. Figure 32 gives the relaxation rate

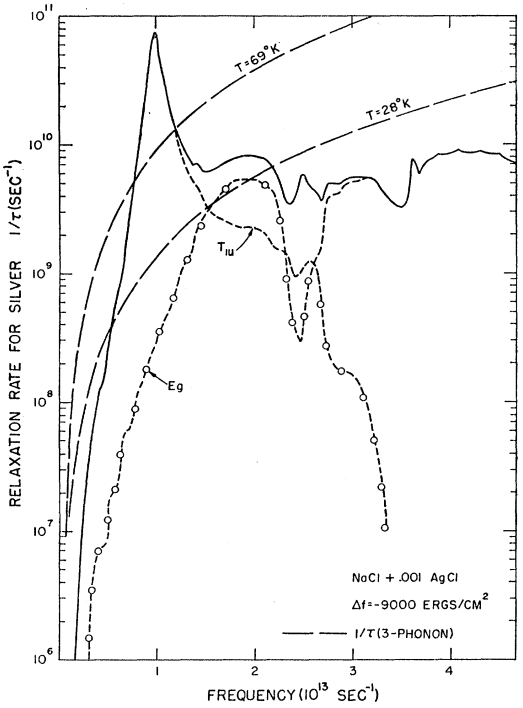

FIG. 32. Total relaxation rate for phonon scattering from silver impurity in NaCl for one force-constant change. Also shown are the contributions to the total from the E_g and T_{1u} configurations. The long dashed lines are the three-phonon rates from Fig. 15. They are drawn in to indicate when the defects will be important.

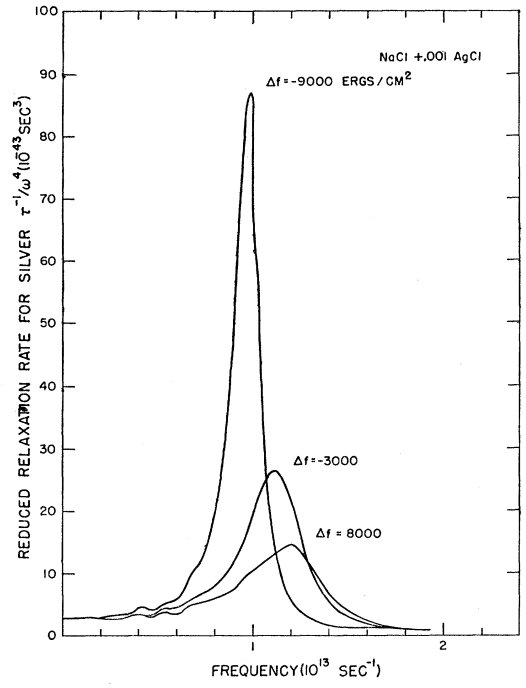

FIG. 31. Reduced relaxation rate for phonon scattering from silver impurity in NaCl for various force-constant changes.

for silver for a concentration of 0.1 mole%. The odd-parity resonance is very strong, so strong that it appears much broader than the previous ones. For this concentration $1/\tau$ (silver) will dominate the three-phonon contribution over the frequency range 0.5×10^{13} to above 2×10^{13} rad/sec at 28°K and below. The peak falls in the middle of the integrand curve at 15°K. The result on the conductivity, as shown in Fig. 7, is similar to that for iodine. In this case, however, the experimental data are much lower. The shapes of the theoretical curves are very similar to those of the experimental ones, but again the predicted scattering at high temperature is too small.

8. Thallium

In the case of TlCl, the mass of the Tl^+ ion is much greater (204 amu) than the sodium mass, and also the lattice constant of 3.83 Å is considerably greater than NaCl, being comparable to CsBr and CsI. Its compressibility, however, of 4.8×10^{-12} cm^2/dyne is fairly close to that of NaCl indicating that the change in force constant should be small. Calculations on our simple model shown in Table III indicates a relatively large change of around 45 000 ergs/cm^2, but this is undoubtedly too high.

Figure 33 shows the reduced relaxation rates for thallium for both $\Delta f = 10\,000$ and 50 000 ergs/cm^2. The

[56] R. Weber, Phys. Letters **12**, 311 (1964).

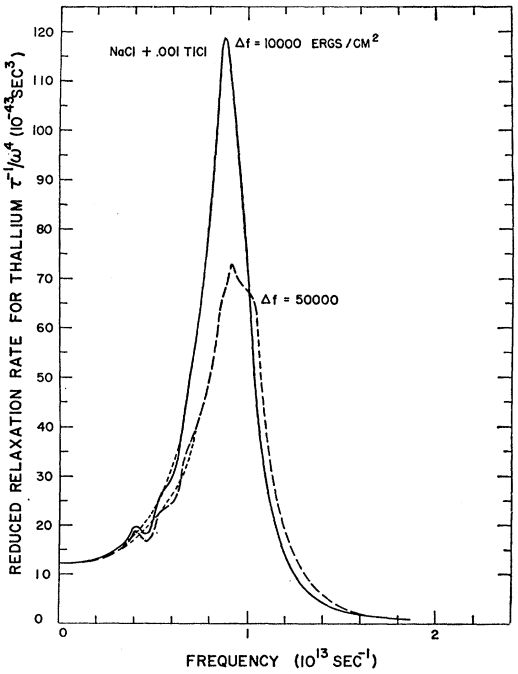

FIG. 33. Reduced relaxation rate for phonon scattering from thallium impurity in NaCl for various force-constant changes.

peak for $\Delta f = 10\,000$ is about the same height and position as that of silver, but the total contribution to $1/\tau_c$ is over a broader frequency range. This will be more important at the lower temperatures where the integrand curves are sharper.

The peak is a true odd-motion resonance at $\omega = 0.9 \times 10^{13}$ rad/sec which arises from the fact that in Eq. (24a) for the real part of the determinant, ΔM is so large that the third and fourth terms override the small positive frequency dependence contained in the $\mathrm{Re}G_{22}$ factor of the second term. It is not due to any particular element of the odd configuration.

The calculated curve in Fig. 8 is for 100 ppm Tl, the experimental curve for 5 ppm. The reason for this is that we originally overestimated the thallium content of our crystal and only recently learned the correct value, too late to re-do the calculation. It is now clear that Tl^+ is a very strong scatterer of phonons, particularly below 10°K. One suspects a strong resonance near 0.3×10^{13} rad/sec, and Fig. 33 suggests that Δf might have to be close to zero or negative. From our study of F^- and Cu^+ (to be discussed next) we can say that such a resonance should be too narrow to yield the necessary conductivity depression, but we would predict a far-infrared absorption band at about 15 cm^{-1}.

9. Copper

Since copper, like silver, has a known infrared absorption band,[57] the change in force constant was determined from this instead of from the compressibility. The absorption band is at 23.7 cm^{-1} and the force-constant change which gives an odd-parity configuration resonance is $\Delta f = -15\,050$ ergs/cm². This value of Δf is close close to $-f_0$, which means that the lattice is almost unstable.

The resonance is the same as that shown theoretically by fluorine and silver, i.e., a "22-resonance," so the plots of the determinant and reduced relaxation rates are not shown here. The total relaxation rates for a concentration of 0.1 mole% is shown in Fig. 34.

Figure 9 shows the comparison between the theoretical calculations and the experimental data. The concentration as determined by analysis is 1.4×10^{-4} mole fraction. The theoretical curve corresponding to this concentration shows very little deviation from the pure curve. The heavier concentration of 1.5×10^{-3} mole fraction is included just to see if a dip will appear at higher concentration where the defect rate will be larger compared to the three-phonon rate.

VI. CONCLUDING REMARKS

It is clear that although the theory predicts resonance-type scattering at the proper frequencies, some improvements must be incorporated to give the proper strengths to the scattering. One important improvement would be a more sophisticated model of the defect which

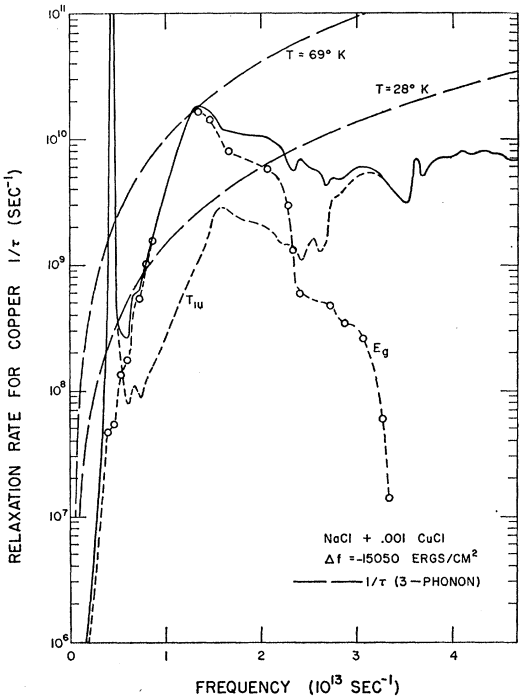

FIG. 34. Total relaxation rate for phonon scattering from copper impurity in NaCl for one force-constant change. Also shown are the contributions to the total from the E_g and T_{1u} configurations. The long dashed lines are the three-phonon rates from Fig. 15. They are drawn in to indicate when the defects will be important.

[57] R. Weber and P. Nette, Phys. Letters **20**, 493 (1966).

would allow both noncentral force changes and long-range strain effects. The extent of the strain field around the impurity was the subject of considerable investigation by Zhurkov and Oskotskii.[55] They studied the impurities Ag^+, Br^-, Li^+, K^+, I^-, and Rb^+ in NaCl from both an experimental and theoretical standpoint. Table IV reproduces their experimental results in the form of the number of sodium ions within a distortion zone whose outer limits are fixed by experimental resolution. Also placed in the table is the percentage difference between the lattice constant of the host lattice and that of the impurity lattice. This is another indication of the size of the distortion zone and allows our placement of the fluorine impurity which they did not measure. The impurities are listed in order of increasing distortion zone. Rubidium is not included due to the concentration difficulties discussed above, and copper and thallium are not included, since CuCl and TlCl have different lattice structures (ZnS and CsCl, respectively).

It is clear that our best fit to our data is attained for silver, which has the smallest distortion zone. The next best fits are attained by bromine and lithium. The lithium fit is better at high temperatures, and bromine is considerably better at low temperatures. The fits for the three impurities, K^+, I^-, and F^-, having the largest distortion zones, are the poorest. Potassium has a very poor high-temperature fit while fluorine has a very poor low-temperature fit, and the analysis for iodine predicts much too strong scattering over the entire range.

It appears, then that there is some correlation between the success of our analysis and the size of the strain field about the defect, so that is is hoped that by expanding the model to include these effects, a much better fit would be achieved.

A problem similar to that of long-range strains is that of distant force-constant changes produced by electric effects. If one treated the impurity ion as well as the lattice consistently in the shell model, which we have not done, one would have to allow for changes in the shell parameters of the impurity. This would produce long-range force-constant changes and keep the perturbation matrix Γ from being localized near the impurity ion.

In the case of Cu^+ and perhaps also F^- and Tl^+ the resonance lines used in the calculation of τ^{-1} are too narrow to explain the experimental curves. These low-frequency phonon resonances should broaden very quickly with increasing temperature due to anharmonic interactions with other phonons. One can see this happening quite clearly in the infrared data of Weber and Nette on NaCl:Cu^+.[57] One should then put the proper thermally broadened peak into the resonance part of τ^{-1}. We intend to do this in future work.

TABLE IV. Size of distortion zone around the impurities.

Impurity	No. of Na^+ ions within the zone	$(r_i-r_0)/r_0$ (%)
Ag^+	115	−1.42
Br^-	290	5.93
Li^+	450	−8.85
K^+	740	11.5
I^-	760	14.8
F^-		−17.9

Another important improvement would be to find better relaxation rates for the three-phonon processes. They would probably not be as smooth a function of frequency as the expression we used, especially near the Van Hove singularities. These might yield better high-temperature fits under the frequency-averaged scheme used here. If the relaxation rates could be found for individual phonons, the conductivity could be obtained as a sum over individual phonons without the somewhat artificial averaging of all of the terms over the frequency surfaces. At this stage it might also be possible to solve the Boltzmann equation by an iteration scheme, thus doing away with the relaxation time approximation and allowing for interference between the various scattering mechanisms.

ACKNOWLEDGMENTS

We are grateful for the assistance of R. A. Cowley and the Chalk River group in sending us the computer program for the shell-model calculations and for the assistance of T. Timusk in the early stages of the programming.

We would also like to thank G. De Pasquali, V. G. Mossotti, and M. Duggan for their analysis of some of the crystals. The help of C. K. Chau and G. E. Moore in measuring the thermal conductivity of the thallium- and copper-doped samples is greatly appreciated.